COINCIDENCE METHODS
FOR
DETERMINING SCINTILLATION COUNTER EFFICIENCY

by

JOHN DUNCAN HEPBURN

B.Sc., The University of British Columbia, 1965

A THESIS SUBMITTED IN PARTIAL FULFILMENT OF

THE REQUIREMENTS FOR THE DEGREE OF

MASTER OF SCIENCE

IN THE DEPARTMENT OF

PHYSICS

We accept this thesis as conforming to the required standard

THE UNIVERSITY OF BRITISH COLUMBIA

June, 1967

In presenting this thesis in partial fulfilment of the requirements for an advanced degree at the University of British Columbia, I agree that the Library shall make it freely available for reference and study. I further agree that permission for extensive copying of this thesis for scholarly purposes may be granted by the Head of my Department or by his representatives. It is understood that copying or publication of this thesis for financial gain shall not be allowed without my written permission.

Department of PHYSICS

The University of British Columbia
Vancouver 8, Canada

Date July 4, 1967

ABSTRACT

The efficiency of a 4" x 5" NaI(Tl) scintillation counter for detecting gamma-rays has been measured by a number of experimental techniques, and the results compared with the efficiencies predicted from total absorption cross sections. The experimental techniques involve coincidence measurements of the cascade gamma-rays from a Co-60 source (1.173 MeV and 1.333 MeV), and from the reaction $B^{11}(p\,\gamma\,\gamma)C^{12}$ (4.43 MeV and 11.68 MeV). The Co-60 measurements also lead to knowledge of the absolute strength of the sources. For both cascades it was necessary to know the angular correlations between the radiations; for the reaction $B^{11}(p\,\gamma\,\gamma)C^{12}$ a separate investigation of this correlation was made using a 180 KeV accelerator. Computer programs were written to analyze the experimental data, and to calculate the theoretical efficiency estimates, taking into account the collimator and shield geometry.

The results of this work define the efficiency of the scintillation counters to better than 5% for a number of gamma-ray energies and a specific geometry. On the other hand, the efficiencies based on the total number of counts in the observed spectra were 20 percent to 40 percent higher than the theoretical efficiencies. The departures from theory depend on the gamma-ray energy and the geometry of the shielding and collimators in such a way that it is not possible to provide a simple basis for relating theoretical efficiencies to the experimental data.

TABLE OF CONTENTS

TABLE OF CONTENTS (cont.)

LIST OF FIGURES

LIST OF TABLES

ACKNOWLEDGEMENTS

I wish to thank Dr. G. M. Griffiths for his untiring supervision of the work described in this thesis, and his assistance in the writing of this report.

It has been my good fortune to have the help of Mr. M. Olivo on many aspects of this work. I am grateful for the philosophical, theoretical, and technical discussions we held. I also thank him for the use of his equipment, and his assistance in operating it.

The assistance of the members of the Nuclear Physics Group and the Van de Graaff technical staff is appreciated.

Finally, I would like to thank my parents and family for their encouragement and support during the course of this work.

CHAPTER I

INTRODUCTION

1.1. General Introduction

In nuclear physics, the detection of gamma rays is a powerful tool for the study of nuclear energy levels and the transition probabilities between the levels. Since the electromagnetic interaction is well known and is much weaker than the nuclear force, information about radiative processes can lead directly to knowledge about either the motions of single nucleons in the nuclei, or the collective motions of several nucleons. In many cases strong selection rules based on conservation laws make electro-magnetic transitions very sensitive to the details of nuclear structure.

An ideal gamma-ray detector would have both a high efficiency and good energy resolution. Prior to the discovery of the scintillation counter, gamma-ray measurements made with Geiger counters had a relatively low efficiency and practically no energy resolution. Energies were determined, with limited accuracy, by tedious absorption methods. Good energy resolution was possible by measuring conversion lines with beta-spectrometers, but the efficiency was low. Since 1948 scintillation counters have been used for quantitative measurement of gamma-ray energies and fluxes, with moderate energy resolution and high efficiency. The discovery of lithium-drifted germanium detectors has recently provided another method

of measurement, with high resolution but as yet low efficiency. Because of these properties, the detectors allow different aspects of gamma-ray spectroscopy to be studied. Typical counters are compared in Table 1. Note that intrinsic peak efficiency is defined here as the ratio of the number of gamma-rays detected in the photopeak by the counter, to the number of gamma-rays incident on the counter face.

TABLE 1.

Comparison of Detectors for 1.33 MeV Gamma-Rays

Type of Detector	Dimensions	Energy Resolution	Intrinsic Peak Efficiency
Tl-activated NaI scintillation counter	5" dia. x 4" deep	85 KeV, 6.3%	38%
Li-drifted Ge*	1.67 cc., 0.5 cm. deep	5 KeV, 0.4%	0.5%

* data supplied by Dalby, 1966.

In the present work, measurements of the absolute efficiency and the spectrum shape have been made for thallium-activated sodium iodide crystals.

1.2. Interaction of Gamma-Rays with Matter

Three main processes describe the interaction of gamma-rays with matter. At low gamma-ray energies ($\lesssim 0.5$ MeV), the photo-electric effect predominates for all but the lowest atomic number materials. In this process all the energy of an incident gamma-ray is transferred to an atomic electron, which

then slows down by transferring the energy it has received to the crystal lattice of the phosphor. For gamma-ray energies around 1 MeV, the most important process is the Compton effect. Here part of the energy is transferred to the atomic electron; the remainder goes off as a lower energy gamma-ray. The cross-section and energy division depend on the initial energy, and the angle of scattering. At energies above 1.02 MeV the photon energy can be converted into an electron-positron pair which share the energy. In order to conserve momentum, this pair production takes place in the field of the nucleus, with small contributions from the atomic electrons at higher incident photon energies. The energy dependence of the three interaction cross-sections is shown in Figure 1.

A fraction of the energy transferred to the electron and then to lattice excitation is emitted in the form of light as the lattice returns to equilibrium. This fluorescent light leaves the transparent phosphor at one end to enter a photomultiplier. The electron avalanche knocked from the anode of the photomultiplier is amplified by the series of dynodes and collected at the first collector electrode. The output pulse is proportional to the amount of light produced when the electrons are stopped by the phosphor; this is in turn proportional to the energy of the incident gamma-rays. Since each of the absorption processes leads to a characteristic electron energy spectrum, the scintillation counter produces a complex

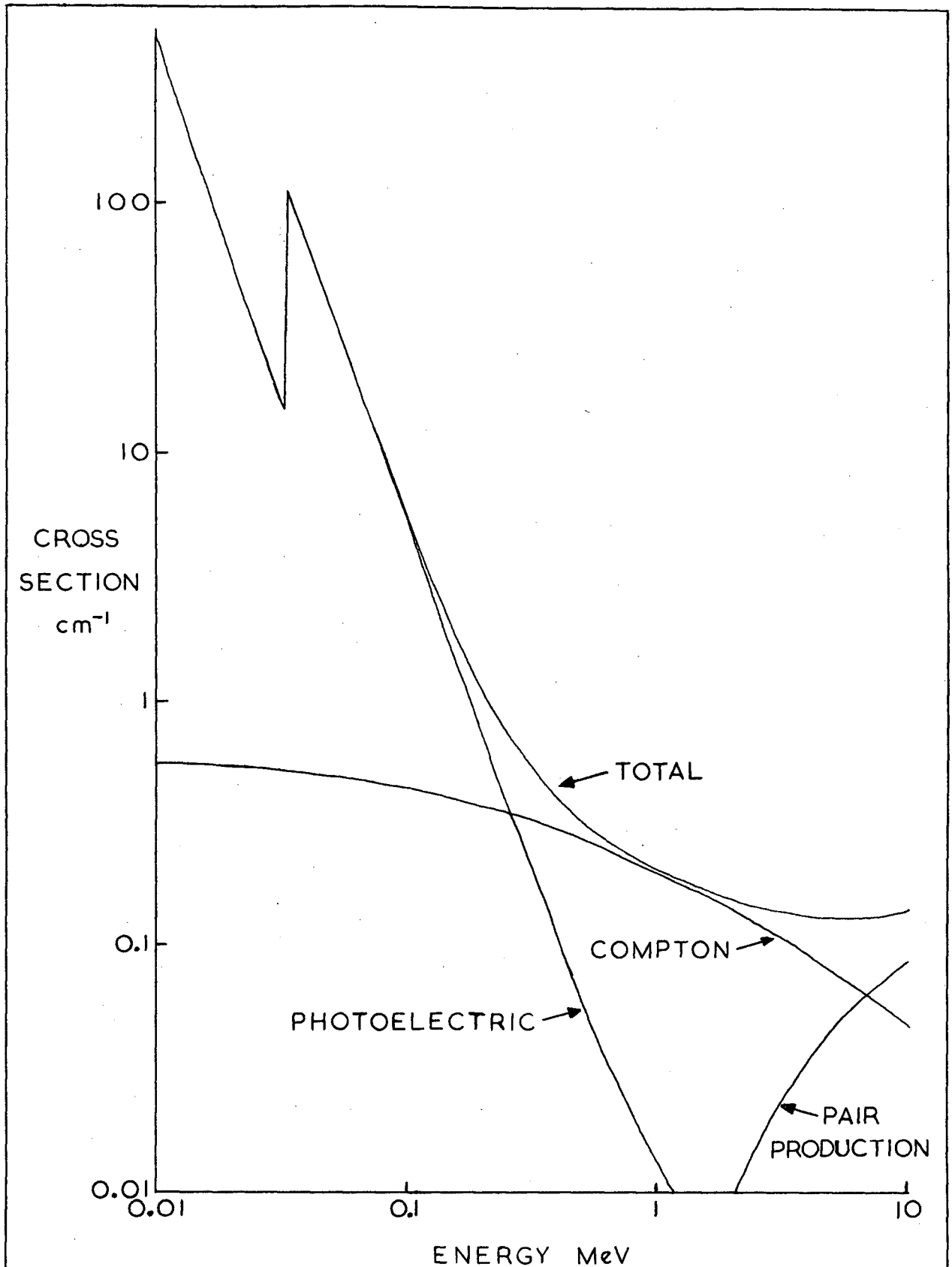

FIGURE 1. Absorption cross sections in thallium-activated sodium iodide, showing the total absorption, and components due to the Compton, photoelectric, and pair production processes. Data from Grodstein (1957).

spectrum of pulse heights.

For quantitative measurement of gamma-ray fluxes and energies, the shape of the scintillation counter (phosphor plus photomultiplier) spectrum must be known. The efficiency of a gamma-ray detector is defined here as the ratio of the number of counts in a specified region of the experimental spectrum to the number of gamma-rays emitted by the source. A knowledge of the spectrum shape is essential for the necessary spectrum integrations. As shown above, the spectrum from a single gamma-ray line is complex, due to the interation mechanisms. In addition, other primary and secondary effects combine to make interpretation of the lower energy part of such a spectrum difficult, if not impossible. Primary processes which interfere are:

(a) presence of other gamma-ray lines of higher or lower energy.

(b) background from the surrounding materials and cosmic rays.

(c) backscatter from other parts of the apparatus.

The secondary processes are:

(a) Bremsstrahlung from the atomic electrons in the phosphor

(b) Compton spectrum from secondary electrons

(c) escape, from the phosphor, of the secondary photons and/or electrons

(d) reabsorption of Compton photons and annihilation quanta.

The presence of these effects prevents the use of a specific relation between the primary processes and the observed spectrum shapes.

1.3. The Background of the Experiment

A theoretical estimate of detector efficiency can be made using the total absorption law. These cross-sections are well known, and are readily available in the literature (Grodstein, 1957). This theory is limited to primary interactions, and cannot calculate the probability of a specific energy transfer. For this reason the entire spectrum shape should be known. The present work involves an attempt to relate the total absorption theory to the experimental spectra of several gamma-rays.

In the UBC Nuclear Physics laboratory measurements of the angular distribution and absolute cross-sections of the reaction $D(p,\gamma)He^3$ are being made using the two NaI(Tl) scintillators as gamma-ray detectors. For this work, and any subsequent work of this type, the absolute detection efficiency for these detectors must be known for a variety of gamma-ray energies.

In an MSc thesis dated October, 1964, J. L. Leigh (1964) discussed the theoretical and experimental gamma-ray

detection efficiencies for a single 3" x 3" NaI(Tl) detector for gamma-ray energies from 0.5 to 12 MeV. However some of his results, notably at 11.68 MeV, did not agree with the total absorption theory.

The present work extends the method to two 5" x 4" NaI(Tl) crystals. In addition, two methods of determining the counter efficiency by means of coincident counts in the detectors are developed. These coincidence methods require gamma-ray sources that have a gamma-gamma cascade. The work involves the use of counters with collimators giving lower background and better defined spectrum shapes.

CHAPTER II

EXPERIMENTAL PROCEDURES

2.1. The Detectors

The gamma-ray detectors used here were two 5" ±0.005" diameter by 4" ±0.005" deep cylindrical NaI(Tl) crystals, obtained from Harshaw Chemical Company. The low-background stainless steel mounting was used, in which the gamma-ray window was 0.019" ± 0.005" thick. Using the total absorption cross sections from Grodstein (1957) the absorption results in Table 2 were obtained.

TABLE 2.

Probabilities of Absorption of Gamma-Rays in 4" of NaI(Tl) Phosphor

Gamma-ray Energy	Probability of Absorption
0.5	0.97
1.0	0.88
2.0	0.78
5.0	0.73
10.0	0.74
20.0	0.80

The gamma-ray detectors are mounted in identical lead shields and collimators (see Figure 2). The tapered collimators achieve three things:

(1) background counts resulting from gamma-rays entering the front face of the crystal are reduced considerably.

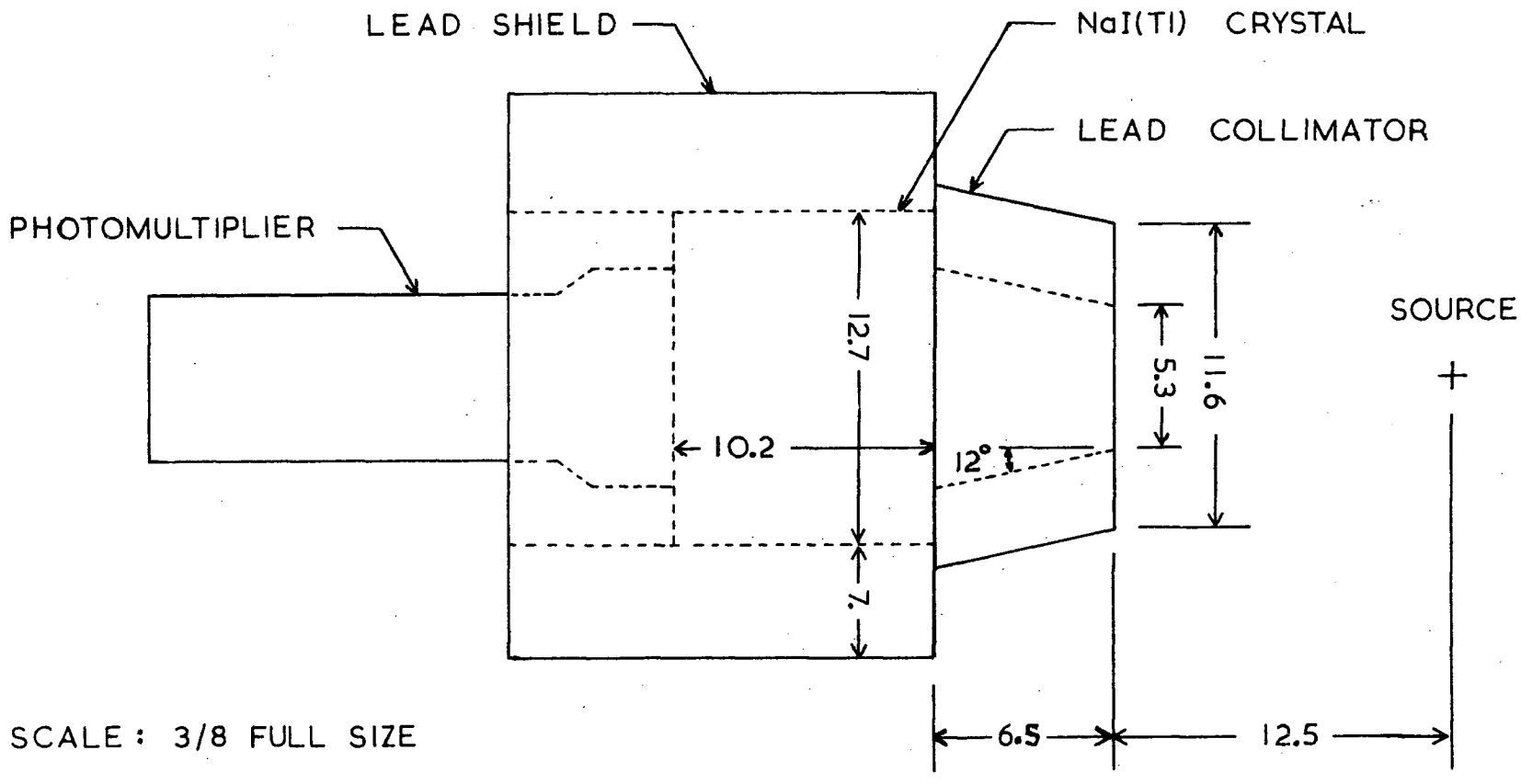

FIGURE 2. A schematic diagram of the counter geometry, with dimensions in centimetres. Table 5 gives the exact dimensions and tolerances.

(2) the edge effects of the crystal are reduced; in other words the active region of the NaI(Tl) crystal is completely surrounded by more NaI(Tl).

(3) the total efficiency, or count rate, is reduced somewhat, but the ratio of totally absorbed to partially absorbed gamma-rays is improved.

These effects are investigated in Section 4.7 of this thesis, while the criteria used to design the collimators are discussed in Section 4.3.

2.2. The Electronic System

The NaI(Tl) crystals are mounted on 3-inch RCA 8045 photomultipliers, which were usually operated at 1100 volts. The voltage signals from the photomultipliers are matched to 50 ohm line by preamplifiers, which are designed to shape a typical pulse from the photomultiplier into a form compatible with the low level input of the Nuclear Data ND 120 and ND 160 kick-sorters used in the spectrum analysis. The preamplifier circuit is displayed in Figure 3. For the 1.33 MeV gamma-rays from a Co-60 source, the output of the preamplifier has the following characteristics across 50 ohms: amplitude = 36 mv., rise time = 0.6 μsec., and fall time = 18 μsec. A 15 MeV gamma-ray produces an 0.42 volt pulse. A list of commercial electronic units used for the experimental analysis is given in Table 3. In the following description of the electronic

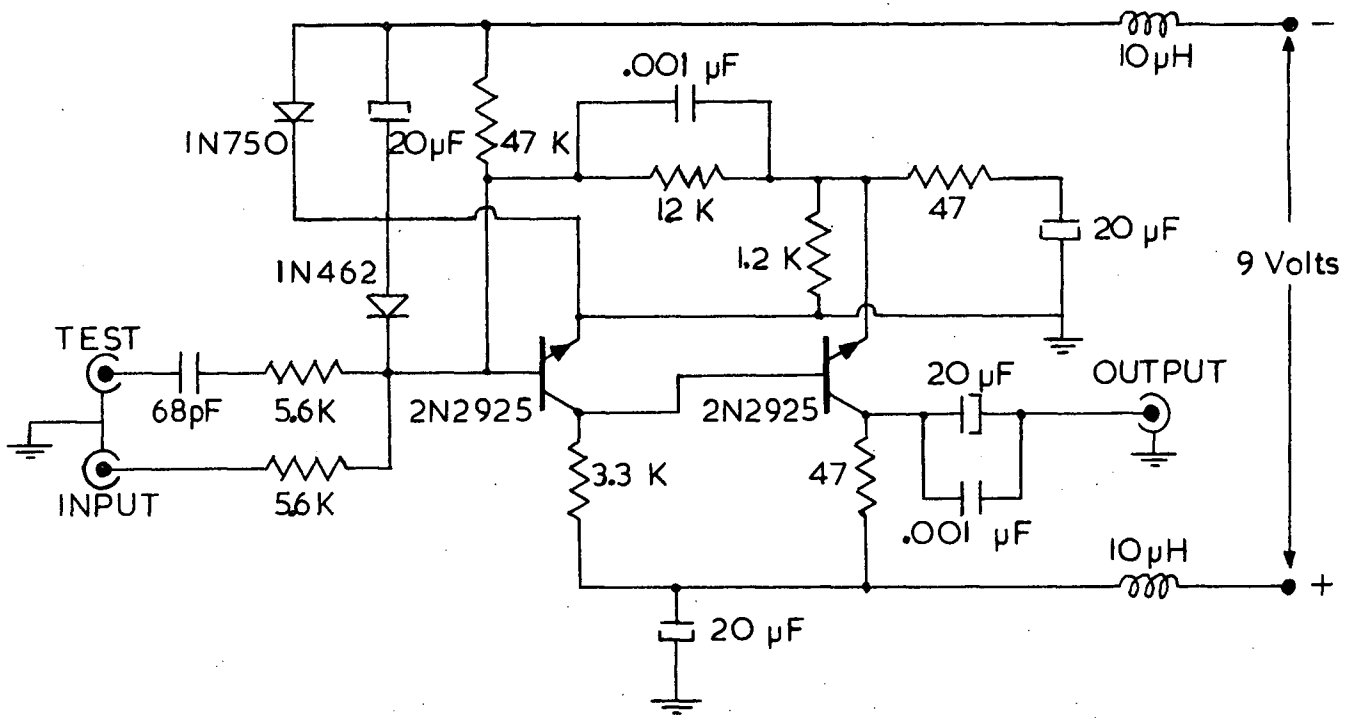

FIGURE 3. Circuit diagram of the detector preamplifier. The output pulses are negative. The 10 μH inductors are used if more than one preamplifier is used with the same power supply.

arrangement, the numerals in parentheses refer to this table. A schematic diagram of a typical electronic arrangement is shown in Figure 4.

For coincidence measurements the preamplifier signals were amplified by double delay line amplifiers (1). Pulses in a chosen range were selected by single channel analyzers (2), whose outputs were logic pulses of 55 nanoseconds duration and 4 volts amplitude. These pulses triggered pulse generators (6), the outputs of which were accepted by a fast coincidence unit (4). The coincidence resolving time, usually selected at 0.5 microseconds, was adjusted by varying the pulse generator output pulse widths. The output of the coincidence unit triggered a pulse generator (6), which opened the kicksorter gate for 5 μsec. Random coincidences were measured by delaying one logic pulse and putting the delayed pulse into a second coincidence unit (4). Several scalers (3,5) were used to record counts at various points in the circuit.

The entire electronic system was checked for linearity using a pulse generator which consisted of a stable D.C. supply, an accurate linear potentiometer, and a 60 cps mercury switch. The pulses from the pulse generator, shaped to simulate pulses from the photomultiplier, were injected into the preamplifier input in order to assess the linearity of the system. This pulse generator was also useful for relating the single channel analyzer settings to a desired energy range,

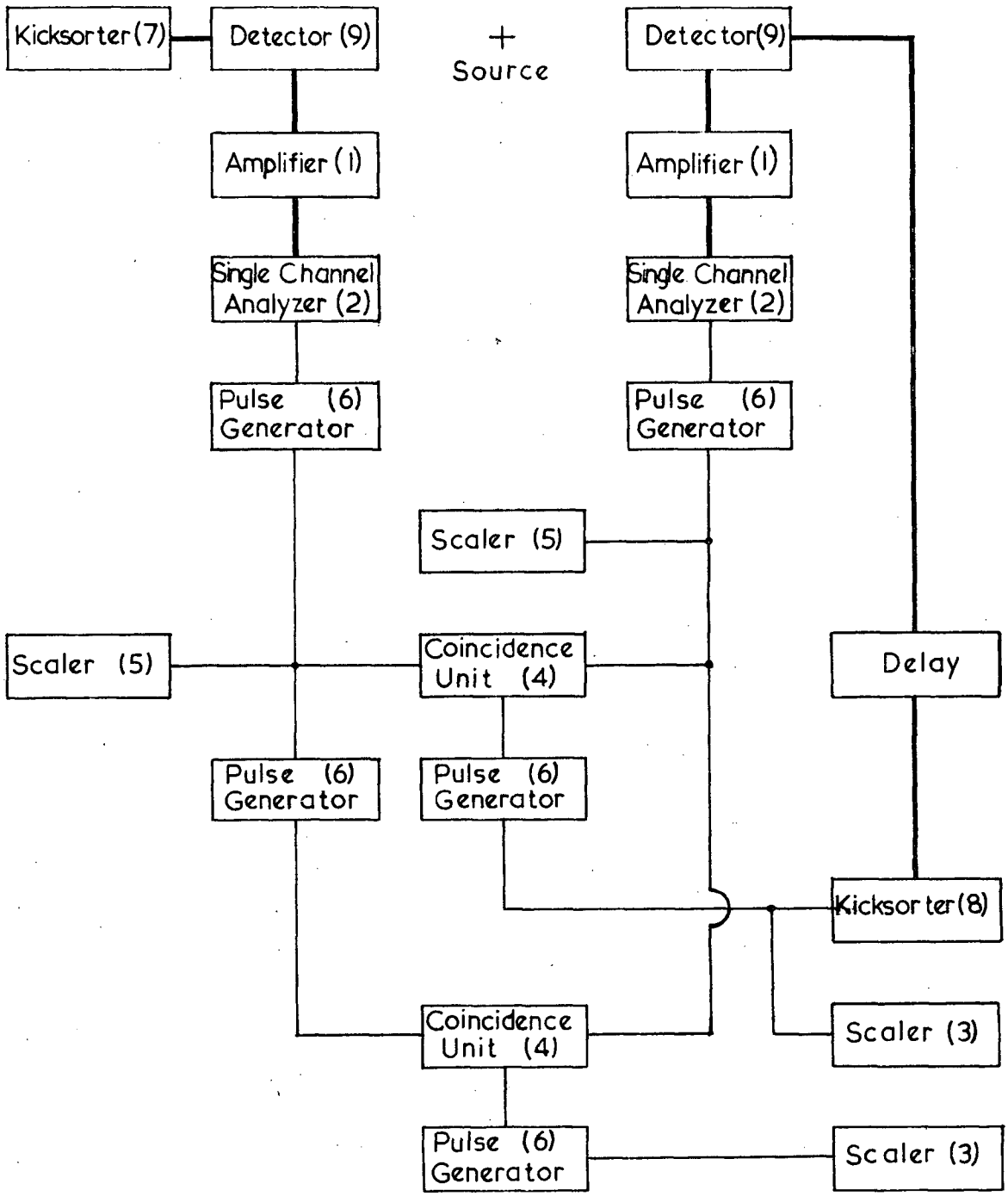

FIGURE 4. Block diagram of a typical electronic arrangement. The numbers in parentheses refer to the commercial units listed in Table 5. The bold lines represent linear electronic channels.

TABLE 3.

A List of Commercial Electronic Units Used

In the Electronic Arrangement

1. Sturrup Model 1410 linear amplifier
   (Canberra Industries, Middletown, Conn.)

2. Sturrup Model 1435 timing single channel analyzer
   (Canberra Industries, Middletown, Conn.)

3. Sturrup Model 1470 scaler
   (Canberra Industries, Middletown, Conn.)

4. LRS Model IIIB 3-fold logic unit
   (LeCroy Research Systems Corp., Irvington, N.Y.)

5. ORTEC Model 430 scaler
   (Oak Ridge Technical Enterprises Corp., Oak Ridge, Tenn.)

6. Datapulse Model 101 and 106A pulse generators
   (Datapulse Inc., Inglewood, Calif.)

7. Nuclear Data ND 120 512 channel analyzer
   (Nuclear Data Inc., Palatine, Calif.)

8. Nuclear Data ND 160 dual parameter analyzer
   (Nuclear Data Inc., Palatine, Calif.)

9. U.B.C. detector assembly, using 5" x 4" NaI(Tl) crystals
   (Harshaw Chemical Co., Cleveland, Ohio), with
   RCA 8045 3-inch photomultipliers, and U.B.C.
   preamplifiers.

as seen on the kicksorter.

The counting rates in the experiments were sufficiently low that the coincidence dead time losses were less than one percent. The kicksorter dead times were energy dependent; the relationship is of the type $t_d = A + B \times \text{energy}$. For the Nuclear Data kicksorters A is of the order of 25 μsec., while B is about 0.5 μsec per channel. Use of internal kicksorter live times, together with an external clock, enabled measurement of the dead time corrections.

The spectra from the two gamma-ray detectors were analyzed in the two kicksorters mentioned previously. The ND 120 is a one dimensional, 512 channel pulse height analyzer, and the ND 160 is a two dimensional, 4096 channel analyzer. Both kicksorters were used in a one dimensional manner, with counts per unit energy interval versus energy as the output information.

It was found, by repeated linear pulse generator checks, that the zero energy intercept for the experimental spectra was constant, and that the gain was stable to within a few percent, over a 12 hour period. However, it was difficult to reproduce a given gain and zero from one experimental run to the next.

2.3. Data Analysis and Computations

The differences in the gains and energy zeros of the

experimental spectra were removed using a computer program written to gain shift experimental spectra from the given gains and energy zeros to the desired gains and energy zeros. The program also enabled the user to analyze simultaneously up to five spectra stored in the computer memory. This data analysis, as well as the calculations of the theoretical efficiency estimates described in Appendix A, was done on the UBC Computing Center facility, an I.B.M. 7040 computer.

Several programs were written for use with the Nuclear Physics Group computer, a Digital Equipment Corporation PDP-8. The topics investigated here included spectrum integration, statistical error calculations, several types of gamma-ray absorption computations, and manipulation of Legendre Polynomial series.

CHAPTER III

METHODS FOR DETERMINING COUNTER EFFICIENCY

3.1. Coincidence Method I

If a gamma-ray source emits two gamma-rays in cascade, information about the efficiency of the counters can be obtained from ratios of the coincidence counting rate to the single counting rate. In general, there are two choices for setting the energy windows; each counter can accept only one of the gamma-rays, or both counters can accept both gamma-rays. The different relations between the theoretical efficiency and the experimental spectrum which apply for these cases are discussed below.

Experimentally, the regions of interest in the energy spectrum are selected by means of energy biases in the single channel analyzers. Since the biases are difficult to set exactly, and because of the possibility of electronic drift, the biases should be selected to lie in an energy-insensitive region of the spectrum. The problem of setting experimental energy biases can be partially eliminated by setting both energy windows to cover the range from as close to zero energy as possible, to an energy above the higher energy gamma-ray. This allows the whole spectrum of both gamma-rays to be recorded in both detectors. This case is discussed below.

Let N_i be the number of gamma rays detected in counter i, N_c be the number of gamma-ray coincidences between the counters, and N_o be the number of cascade events in the source. If ϵ_{ij} is the detection efficiency of counter j for the i^{th} gamma-ray in the cascade, we have

$$N_1 = (\epsilon_{11} + \epsilon_{21}(1 - \epsilon_{11}))N_o$$

$$N_2 = (\epsilon_{12} + \epsilon_{22}(1 - \epsilon_{12}))N_o$$

where the factors $(1 - \epsilon_{11})$ and $1 - \epsilon_{12})$ account for the cases when both gamma-rays are detected together in a single counter. These factors are in general close to 1. Also

$$N_c = (\epsilon_{11}\epsilon_{22} + \epsilon_{21}\epsilon_{12})N_o F(\theta)$$

Here $F(\theta)$ is the correction due to an angular correlation between the gamma-rays of the cascade, as discussed in Appendix B. Then

$$\frac{N_c}{N_1} = \frac{(\epsilon_{11}\epsilon_{21} + \epsilon_{21}\epsilon_{12})F(\theta)}{\epsilon_{11} + \epsilon_{21}(1 - \epsilon_{11})}$$

If the counters are identical, then $\epsilon_{21} = \epsilon_{22}$ and $\epsilon_{11} = \epsilon_{12}$. The above equation becomes

$$\frac{N_c}{N_1 F(\theta)} = \frac{2\epsilon_{11}\epsilon_{21}}{\epsilon_{11} + \epsilon_{21}(1 - \epsilon_{11})}$$

The term $\epsilon_{21}\epsilon_{11}$ in the denominator can be neglected here, since it represents at worst an 0.5% correction over the gamma-ray energy range of interest. The expression on the left can be evaluated experimentally and compared to the theoretical value of the expression on the right. It should be noted that the right hand side of the equation can be rewritten as

$$\frac{2\epsilon_{11}\epsilon_{21}}{\epsilon_{11}+\epsilon_{21}} = \epsilon_{11}\left(\frac{2}{1+\epsilon_{11}/\epsilon_{21}}\right) = \epsilon_{21}\left(\frac{2}{1+\epsilon_{21}/\epsilon_{11}}\right)$$

For gamma-rays in the energy range 0.1 MeV to 20 MeV, ϵ_{11} and ϵ_{21} have reasonably close values, that is $\epsilon_{11}/\epsilon_{21} \approx 1$. If one assumes $\epsilon_{11} = \epsilon_{21}$ then the expression gives the efficiencies ϵ_{11} and ϵ_{21} directly. In this approximation the true efficiencies are equal and correspond to the average efficiency for the two gamma-rays. ϵ_{11} and ϵ_{21} can still be obtained if one assumes the theoretical value for $\epsilon_{11}/\epsilon_{21}$ and $\epsilon_{21}/\epsilon_{11}$.

The spectra required here are the coincidence spectrum and the spectrum from either one of the counters, referred to as the free spectrum. The coincidence spectrum is formed by opening a gate to the kicksorter from one of the counters with a gate pulse from the circuit which demands a coincidence between both counters. Since both gamma-rays are admitted to both counters (and the subsequent electronics) the coincidence spectrum will be the same shape as the free spectra from the counters. In any spectrum, the number of counts above a given energy bias level is proportional to the total counts in the spectrum. Since the coincidence and free spectra are the same shape, the same bias corresponds to the same fraction of the total counts for both coincidence and free spectrum. Therefore, the ratio of coincidence counts to free counts is independent of the bias. By choosing a convenient

bias, for instance the half energy bias of the lower energy gamma-ray, uncertainties in integrating the lower part of the gamma-ray spectra can be completely eliminated, and a true count ratio obtained.

Since this theory applies to any gamma-ray cascade, there are several experimental reactions available for a check on the theoretical counter efficiency estimates for various gamma-ray energies.

3.2. Coincidence Method II

If the two gamma rays are well separated in energy, a different technique may be used. The assumption here is that the electronic single channel analyzers are set so that each counter 'records' only one of the gamma-rays. Experimentally this introduces the complication that only one of the energy windows can have a zero energy baseline, since the energy windows cannot overlap. Clearly the window set on the lower energy gamma-ray has the zero baseline. In addition, this window will contain counts from the tail of the upper gamma-ray, however these counts cannot contribute to the true coincidence counts. This method rejects legitimate counts which lie below the baseline for the upper gamma-ray window, however this does not affect the measurement of counter efficiency at the lower gamma-ray energy. The efficiency measured for the higher energy gamma-ray is then relative to a bias W, the baseline energy of the upper energy window.

Let N_o be the number of events in the source, N_i be the number of gamma-rays of energy E_i detected in counter i, in the desired energy range. Assuming that $E_1 < E_2$ and that the detection efficiencies are ϵ_1 and ϵ_{2W}, we have

$$N_1 = \epsilon_1 N_o \tag{3.1}$$

$$N_{2W} = \epsilon_{2W} N_o \tag{3.2}$$

$$N_c = \epsilon_1 \epsilon_{2W} N_o F(\theta) \tag{3.3}$$

Where $F(\theta)$ is the angular correlation factor derived in Appendix B. The efficiencies are given by

$$\epsilon_1 = \frac{N_c}{N_{2W} F(\theta)} \tag{3.4}$$

$$\epsilon_{2W} = \frac{N_c}{N_1 F(\theta)} \tag{3.5}$$

Thus this technique leads directly to the efficiency, ϵ_1, of the detectors for the lower energy gamma-ray and to the efficiency, ϵ_{2W}, of the detector for the upper energy gamma-ray to a bias W. If one knows the fraction of counts to any bias X above or below W, then one can use the measured ϵ_{2W} to determine the efficiency to the bias X. Clearly if X is zero, we have the total efficiency of the counter for the gamma-ray.

Assuming that $X < W$ we define N_2^1 as the number of the

higher energy gamma-rays detected by the upper counter as having energies between W and X. Then the number of coincicences lost because of the bias W on the single channel analyzer is

$$N_c' = N_2' \epsilon_1 F(\theta) \tag{3.6}$$

Also we have the results

$$N_2' + N_{2W} = \epsilon_{2X} N_0 \tag{3.7}$$

$$N_c' + N_c = \epsilon_{2X} \epsilon_1 N_0 F(\theta) \tag{3.8}$$

From equations (3.1) and (3.8) we get

$$\epsilon_{2X} F(\theta) = \frac{N_c + N_c'}{N_1}$$

which becomes

$$\epsilon_{2X} F(\theta) = \frac{N_c}{N_1} + \frac{N_2' \epsilon_1}{N_1}$$

$$\epsilon_{2X} F(\theta) = \frac{N_c}{N_1} + \frac{N_2'}{N_1}\left(\frac{N_1 \epsilon_{2X} F(\theta)}{N_2' + N_{2W}}\right)$$

Solving this result for ϵ_{2X} we get

$$\epsilon_{2X} = \frac{N_c}{N_1 F(\theta)}\left(\frac{N_2' + N_{2W}}{N_{2W}}\right)$$

$$\epsilon_{2X} = \epsilon_{2W}\left(\frac{N_2' + N_{2W}}{N_{2W}}\right)$$

Clearly if $X > W$, N_2' is a negative quantity. For the case $X < W$, it is not always easy to determine the shape of the spectrum and thus to find N_2'. For this reason it is not easy to relate experimental efficiencies obtainable for

counts above a given bias to theoretical efficiencies based on total absorption cross sections. As shown by Leigh (1964), the determination of such a spectrum shape is at best an educated guess.

3.3. Standard Source Method

The efficiency of a single counter can be readily measured, if a calibrated source of gamma-rays is available. In the measurements to be described later, a standard Co-60 source was used. The equations for a gamma-ray cascade stated in Section 3.1 apply, namely

$$N_1 = (\epsilon_{11} + \epsilon_{21}(1 - \epsilon_{11}))N_0$$

where ϵ_{ij} is the efficiency of counter j for the i^{th} gamma-ray in the cascade. Here N_0 is the number of cascade events in the source, and N_1 is the number of gamma-rays detected. As before, the approximation $\epsilon_{11} \ll 1$ is used. Since N_0 is accurately known from the source strength, the total efficiency $(\epsilon_{11} + \epsilon_{21})$ is given directly by the counts N_1 in the single counter.

CHAPTER IV

EXPERIMENTAL INVESTIGATION OF THE DETECTOR EFFICIENCIES

4.1. Introduction

The three methods of determining counter efficiency discussed in the previous chapter were used to find the efficiencies of two 5" x 4" NaI(Tl) gamma-ray detectors using two gamma-ray cascades. These were the 1.173 MeV and 1.333 MeV gamma-rays from a Co-60 source, and the 4.43 MeV and 11.68 MeV gamma-rays from the reaction $B^{11}(p\,\gamma\gamma)C^{12}$. Measurements made both with and without the detector collimators are outlined below.

The presence of pulse pile-up in the free spectra taken in the experiments must be considered. The "pile-up" pulses can occur in two ways: the first occurs if the two gamma-rays in one cascade are detected in one counter, the second occurs when two independent gamma-rays from separate decays in the source are detected together. The first type of pile-up produces one large pulse in the counter. The ratio of pile-up pulses of this kind to total free counts is just the average efficiency (as discussed in Coincidence Method I) times the angular correlation factor, a value usually about $1 \pm .5$ percent. The second type of pile-up produces two pulses with a large degree of time overlap, which are accepted by an electronic device as one large pulse. The ratio of pile-up

pulses of the second kind to total free counts is equal to twice the resolving time of the electronic device times the free count rate. Clearly, different electronic devices have different resolving times, so each case must be treated separately. Not all the pile-up pulses are shifted out of the energy range of interest in the experiments, however, so the magnitude of the effect as evaluated above represents an upper limit to the actual corrections necessary. For this reason, the magnitude of the pulse pile-up effects is evaluated for each experimental measurement, but the correction is not made to the stated results.

4.2. The $B^{11}(p\,\gamma\gamma)C^{12}$ Reaction

The reaction B^{11} + p has resonances in gamma-ray yield at proton energies of 0.163, 0.675 and 1.388 MeV. In the present work, only the 163 KeV resonance, with a total width of 7 KeV, was used. Information on the various competing channels for the gamma-ray break-up of the 16.11 MeV excited level of the C-12 nucleus which are produced at the 163 KeV resonance are shown in Table 4 and Figure 5. (unless otherwise stated, the data in this section were obtained from Ajzenberg-Selove and Lauritsen, (1959).) The lifetime of the 4.43 MeV level in C-12 has been measured to be about 5×10^{-14} sec. by both resonance fluorescence (Rasmussen et al, 1958), and by Doppler shift techniques (Devons, 1961). This time is so short compared to the experimental coincidence resolving

times used in this work that one can assume that the cascade of 11.68 and 4.43 MeV gamma-rays that de-excite the 16.11 MeV level of C-12 are emitted at the same time.

TABLE 4.

Competing Channels in the $B^{11}(p\,\gamma\,\gamma)C^{12}$ Reaction, for E_p = 163 KeV

Reaction	Absolute Cross Section	Gamma-Ray Energy
$B^{11}(p\,\gamma_0)C^{12}$	5.5 μb	E_0 = 16.11 MeV
$B^{11}(p\,\gamma_1\,\gamma_2)C^{12}$	152. μb	E_1 = 11.68 MeV E_2 = 4.43 MeV
$B^{11}(p\,\gamma_3)C^{12*}(\alpha)Be^8$	$<$1.8 μb +	E_3 = 6.48 MeV

+ Gregory, 1961

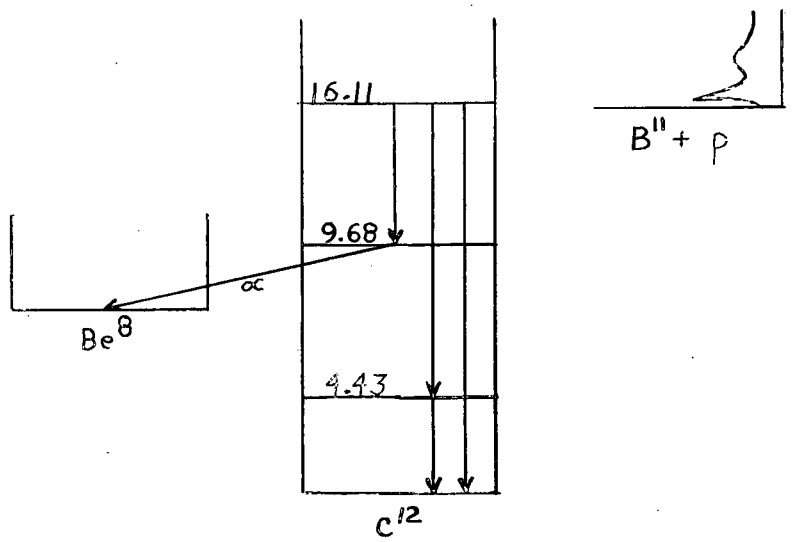

FIGURE 5. Some energy levels in the C-12 nucleus, showing channels in the $B^{11}(p\,\gamma\,\gamma)C^{12}$ reaction.

4.3. The Apparatus

The B^{11} + p reaction was produced with a 185 KeV accelerator having an ORTEC Duoplasmatron ion source. The proton beam was selected from the mass 2 and mass 3 beams by means of a double focussing analyzing magnet. Copper-backed B-11 targets of about 150 $\mu gm/cm^2$ thickness were obtained from Harwell for the experiment. A proton energy of 170 KeV was chosen after an excitation function was found for the 163 KeV resonance. When the targets were indium-soldered on a water-cooled target holder, sustained proton beams of 60 to 80 microamperes could be used. Under such conditions the boron in the beam spot tended to flake off, resulting in a 25 percent loss in gamma-ray yield over a two hour counting period.

The target holder consisted of a 0.125 inch thick copper plate, with 0.082 inch diameter holes for water cooling drilled lengthwise through the copper, every 0.10 inches. The holder could be rotated about a vertical axis, to provide variable angles between the target normal and the incident proton beam.

The two NaI(Tl) gamma-ray detectors were mounted on an angular distribution table which was used in conjunction with the accelerator. The counters, with shielding and collimators, were mounted on rotating I-beams that pivoted around a centre directly under the target chamber.

The dimensions of the collimators were chosen so that for a desired counter face to target distance, the cone defined by the collimator coincided with one defined by the back surface of the NaI(Tl) crystal having its apex at the target spot. The dimensions of the counter assembly are shown in Table 5, while the geometry has been shown in Figure 2.

TABLE 5.

Dimensions of the Counter Assembly

Item	Measurement
collimator half angle	12.0 $\pm$ .05 degrees
minimum collimator inner diameter	5.30 $\pm$ .05 cm
minimum collimator outer diameter	11.63 $\pm$ .05 cm
collimator thickness (perpendicular to the counter axis)	6.54 $\pm$ .05 cm
Table centre to collimator face	12.46 $\pm$ .05 cm
Table centre to crystal face	19.52 $\pm$ .05 cm
crystal thickness	10.16 $\pm$ .02 cm
crystal diameter	12.70 $\pm$ .02 cm
thickness of lead shielding	4.0 cm

4.4. The Results of 4.43 MeV and 11.68 MeV

Since the gamma-ray energies from this reaction are well separated, both coincidence methods could be used to investigate the detector efficiency. The method of analysis

which was applied to the experimental results, including the various corrections, is now discussed.

In all efficiency measurements, the gamma-ray absorption between the point of origin and the NaI(Tl) crystals can be treated as a factor, which is actually the fraction of gamma-rays transmitted, which multiplies the true efficiency of the counters. The gamma-ray losses due to absorption in the counter face, the target chamber, and the target assembly, which are shown in Table 6, were calculated from the total absorption cross sections of Grodstein, (1957). Absorption losses in the target backing and the water-cooled target holder were calculated assuming even layers of copper and water, whose thicknesses represented an average over the actual distribution of these absorbers. The calculations of target holder absorptions were checked by measuring the absorption of 11.68 MeV gamma-rays. These checks are shown in Table 7, where the target angle is defined as the angle between the target normal and the counter axis.

The angular correlation factor necessary was measured experimentally. The theoretical and experimental discussion is given in Chapter VII of this thesis.

Uncertainties in data obtained by integrating pulse height spectra from one energy (usually chosen small with respect to the full energy) to another energy (usually chosen

TABLE 6.

Calculated Absorption Corrections

Absorber	Material	Thickness	Target Angle	Calculated Fraction Transmitted 4.43 MeV	11.68 MeV
target chamber	brass	0.020 ± 0.003 "	--	0.9858	0.9864
counter assembly	stainless steel	0.019 ± 0.0005"	--	0.9630	0.9697
	magnesium oxide	0.09 ± .01 "			
target assembly	copper	0.072 ± 0.005 "	30°	0.9313	0.9358
	water	0.053 ± 0.005 "	45°	0.9165	0.9219
			60°	0.8840	0.8914

TABLE 7.

Target Holder Absorption Measurements,

for E_γ = 11.68 MeV

Target angle	Calculated Fraction Transmitted	Measured Fraction Transmitted
30°	0.9358	0.94 ± 0.02
45°	0.9219	0.93 ± 0.02
60°	0.8914	0.90 ± 0.02

above the full energy) are of two types. The first is the statistical uncertainty in the total counts observed, and the second is the uncertainty in locating the exact channels to correspond to the required energies. These uncertainties can be partly eliminated by choosing the integration limits (and experimental energy biases) to lie in slowly varying regions of the spectra. The background statistical uncertainties were minimized by using long counting times, but the integration uncertainties still exist. Repeated pulse generator checks revealed no significant changes in the electronic gains and discrimination levels during the runs.

Typical numerical values of the uncertainties, which are combined using the root sum square of the components, are:

counting statistics	1.5%
geometry determination	1.5%
spectrum analysis	1.0%
total	2.4%

Assumptions concerning spectrum shape were made in order to find the efficiency results. In all cases where the spectrum of a single gamma-ray was obscured by other gamma-rays, a 'flat tail' was used to approximate the desired shape. The flat tail is drawn parallel to the energy axis, tangent to the unobscured part of the spectrum component of interest. Figure 6 shows a gamma-ray spectrum with the flat tails so drawn. This approximation was used for all free spectra, in

order to remove the effect of the 16.11 MeV and 6.48 MeV gamma-ray spectrum components.

The only results requiring further use of the flat tail approximation are the efficiencies at 11.68 MeV, where the flat tail approach was applied to the 11.68 MeV spectrum also. To find the efficiency to the bias W, the 4.43 MeV component of the free spectrum must be separated from the total, from about 2.0 MeV up to full energy. To derive the full-spectrum efficiency, the entire shape of the 11.68 MeV component must be known. The significance of the flat tail approximation is further discussed in Chapter VI of this thesis.

Wherever possible, the experiments were performed with the counters at right angles to each other; this reduced the possibility of gamma-rays (either primary or secondary) scattering from one crystal into the other.

The double delay line amplifier gains and single channel analyzer baselines could be set so that, when a zero energy baseline was desired, the baseline was actually 200 KeV. When the true counts below this energy level are considered in relation to the total number of counts in the spectra, it is seen that the corrections for counts eliminated by the non-zero baselines are negligible.

A typical free spectrum observed from the reaction

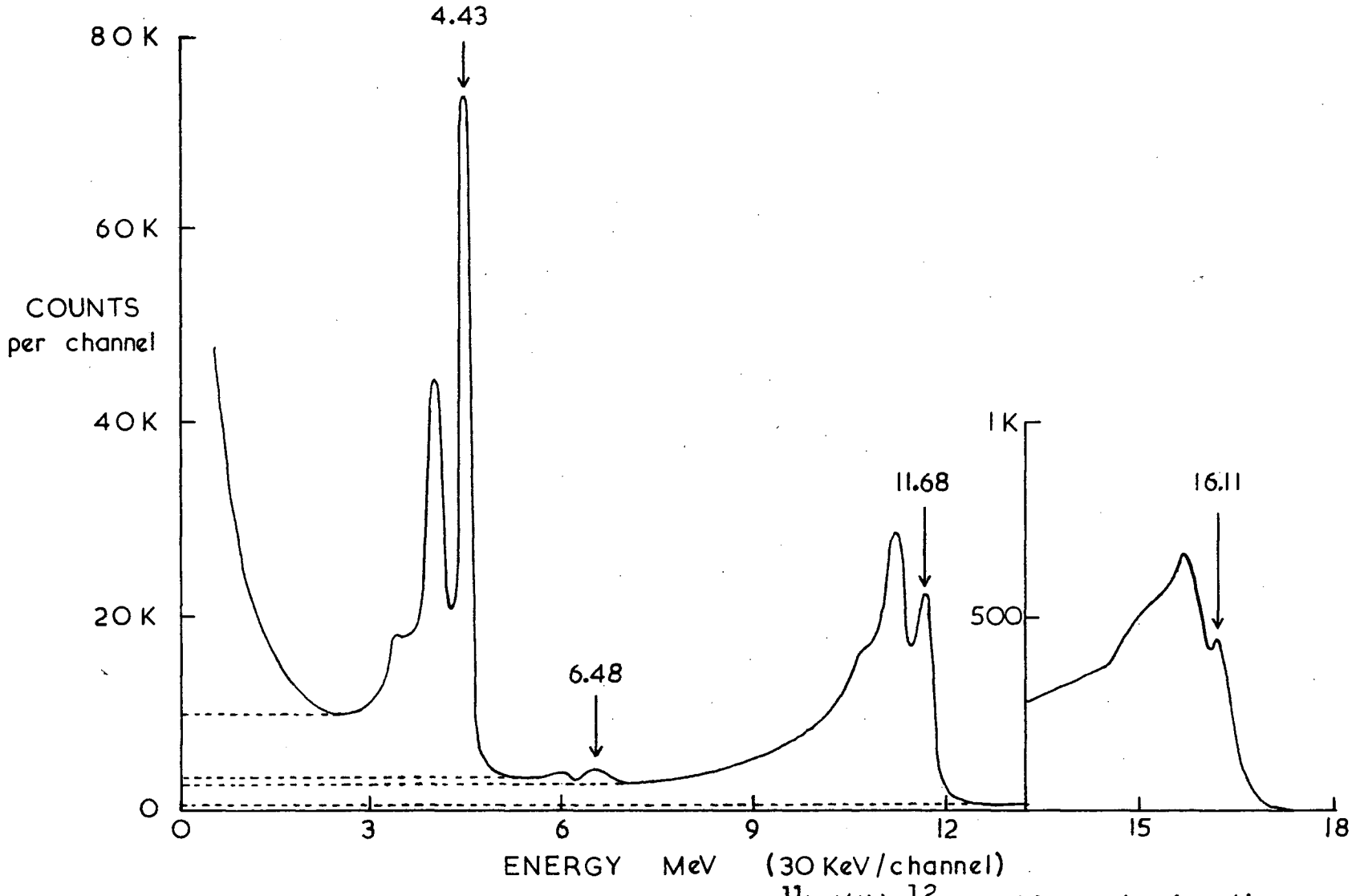

FIGURE 6. A typical spectrum from the $B^{11}(p\gamma\gamma)C^{12}$ reaction, showing the four gamma-ray peaks and the flat tail approximation for each.

is shown, with background removed, in Figure 6. This spectrum was taken in 2.75 hours, with a total collected charge of 0.6 coulombs. Under these conditions the free count rate, including 5×10^3 counts per minute background, was approximately 3×10^5 counts per minute, while the coincidence count rate was about 90 counts per minute, including 4 random coincidences per minute. The pulse pile-up corrections, as discussed in Section 4.1. were found to be 2 percent for a kicksorter resolving time of 2 μsec.; this correction was not made to quoted results.

The numerical results obtained are shown in Table 8. The ratio of efficiencies, $\epsilon_{4.43} / \epsilon_{11.68}$, was obtained by two methods. The first was a direct ratio of the measured efficiencies obtained from coincidence counting, and the second was the ratio of 4.43 to 11.68 MeV gamma-rays detected in one of the free spectra. The values measured for the counter efficiencies are compared to the theoretical estimates of the parameters shown in Table 8. These theoretical values were obtained using the total absorption theory of Appendix A, and the absorption cross sections of Grodstein (1957).

TABLE 8.

Results at 4.43 MeV and 11.68 MeV

Parameter Measured	Coincidence Method	Measured Efficiency	Theoretical Estimate	Percent Deviation
$\frac{2\epsilon_{4.43}\,\epsilon_{11.68}}{\epsilon_{4.43}+\epsilon_{11.68}}$	I	$(1.13\pm0.02)\times10^{-2}$	8.37×10^{-3}	36%
$\epsilon_{4.43}$	II	$(1.16\pm0.02)\times10^{-2}$	8.26×10^{-3}	40%
$\epsilon_{11.68,W}$	II	$(8.89\pm0.17)\times10^{-3}$	n.a.	n.a.
$\epsilon_{11.68}$	II	$(1.19\pm0.02)\times10^{-2}$	8.49×10^{-3}	40%
$\epsilon_{4.43}/\epsilon_{11.68}$	II	(a) 0.97 ± 0.03 (b) 0.96 ∓ 0.02	0.974	(a) $<1\%$ (b) 1%

4.5. Measurements at 1.173 and 1.333 MeV with the Coincidence Method

A Co-60 source was used to provide a second gamma-ray cascade. The Co-60 nucleus decays by β^- emission to the 2.506 MeV excited level of Ni-60, which subsequently decays to the ground state by a cascade of 1.173 and 1.333 MeV gamma-rays, as shown in Figure 7.

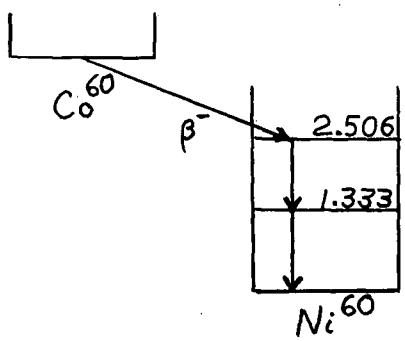

FIGURE 7. The Decay Scheme of Co-60.

The half life of the β^- decay is 5.27 $\pm$ .05 years. (Nuclear Data Tables, 1960). The half life of the intermediate 1.333 MeV level is 8×10^{-12} seconds (Nuclear Data Tables, 1960), and is therefore completely negligible with respect to the experimental coincidence resolving time.

The gamma-rays are isotropically distributed over angles, however there is an angular correlation between the directions of emission of the first and second gamma-rays of the cascade. The angular correlation function, quoted by Frauenfelder and Steffan, in Siegbahn, 1965, is given by

$$W(\theta) = 1.0 + 0.1020\, P_2(\cos\theta) + 0.0091\, P_4(\cos\theta)$$

where θ is the angle between the gamma-ray directions. For the geometry used in the present work, the finite counter solid angle corrections (see Appendix C) change the function to

$$\overline{W(\theta)} = 1.0 + 0.09538\, P_2(\cos\theta) + 0.00725\, P_4(\cos\theta)$$

In determining the scintillation counter efficiency by the coincidence method, this function is used to correct the results for the effects of the correlation between the gamma-rays, as discussed in Appendix B (where the function is represented by $F(\theta)$).

Two different Co-60 sources (those designated #11 and #15 in the laboratory isotope records) were used to measure the detector efficiency with Coincidence Method I. These

sources were chosen because they are sufficiently weak (about 0.5 μc.) that the random coincidence rate, which depends on the square of the source strength, was much less than the true coincidence rate, which is proportional to the source strength. Because the gamma-rays have nearly the same energy, the gamma-ray spectrum components could not be adequately separated by the counters and associated electronics. Therefore, reliable measurements with Coincidence Method II were not possible.

The Co-60 measurements were made using the angular distribution table with the target chamber removed, in order to eliminate gamma-ray absorption and scattering in the chamber walls. The sources were mounted on the center post of the table, and moved up, down, and sideways several centimetres to locate the position of maximum counting rate, corresponding to the source being on the counter axis. The source position is not critical, for a shift of 0.5 cm. from the counter axis reduces the count rate by one percent.

In the experimental runs, the lower bias levels on both single channel analyzers, whose outputs generated coincidence pulses, were set to a level corresponding to 20 KeV. The upper levels were set to 1.6 MeV. For source #15, the single channel counting rate, including the 7×10^3 counts per minute background, was 4×10^4 counts per minute. The coincidence rate was 330 counts per minute, of which 18 counts per minute were random coincidences. The pulse pile-up effect here

totalled 1.2 percent, since for a kicksorter resolving time of 2 μsec., and the count rates present here, the probability of pulse overlap is negligible.

A typical spectrum, taken in a 2 hour run with source #15, is shown in Figure 8. With the counters at 90 degrees to each other, the ratio of coincidence counts to free counts in counter 1, taken in one hour, was

$$\frac{N_c}{N_1 F(\theta)} = \frac{2\,\epsilon_{1.173}\,\epsilon_{1.333}}{\epsilon_{1.173} + \epsilon_{1.333}} = (1.15 \pm .03) \times 10^{-2} \quad \text{for source \#15}$$

$$= (1.14 \pm .03) \times 10^{-2} \quad \text{for source \#11}$$

This value is approximately equal to the average efficiency for one counter for the two Co-60 gamma-rays, assuming the counters to be identical. Using the absorption coefficients from Grodstein (1957), the efficiency factors were calculated to give 0.951×10^{-2} for the theoretical value of the above expression. The large 20 percent difference between the experimental and theoretical values will be discussed in Chapter VI.

The ratio of counts N_c/N_1 should be independent of the energy range over which the spectra are integrated, as long as the same range is used for both the coincidence and free spectra. The ratios given above for source #11 were calculated from the number of counts in the experimental spectrum above a channel number equivalent to an energy of 0.33 MeV; using a lower integration limit of 0.77 MeV the ratio obtained

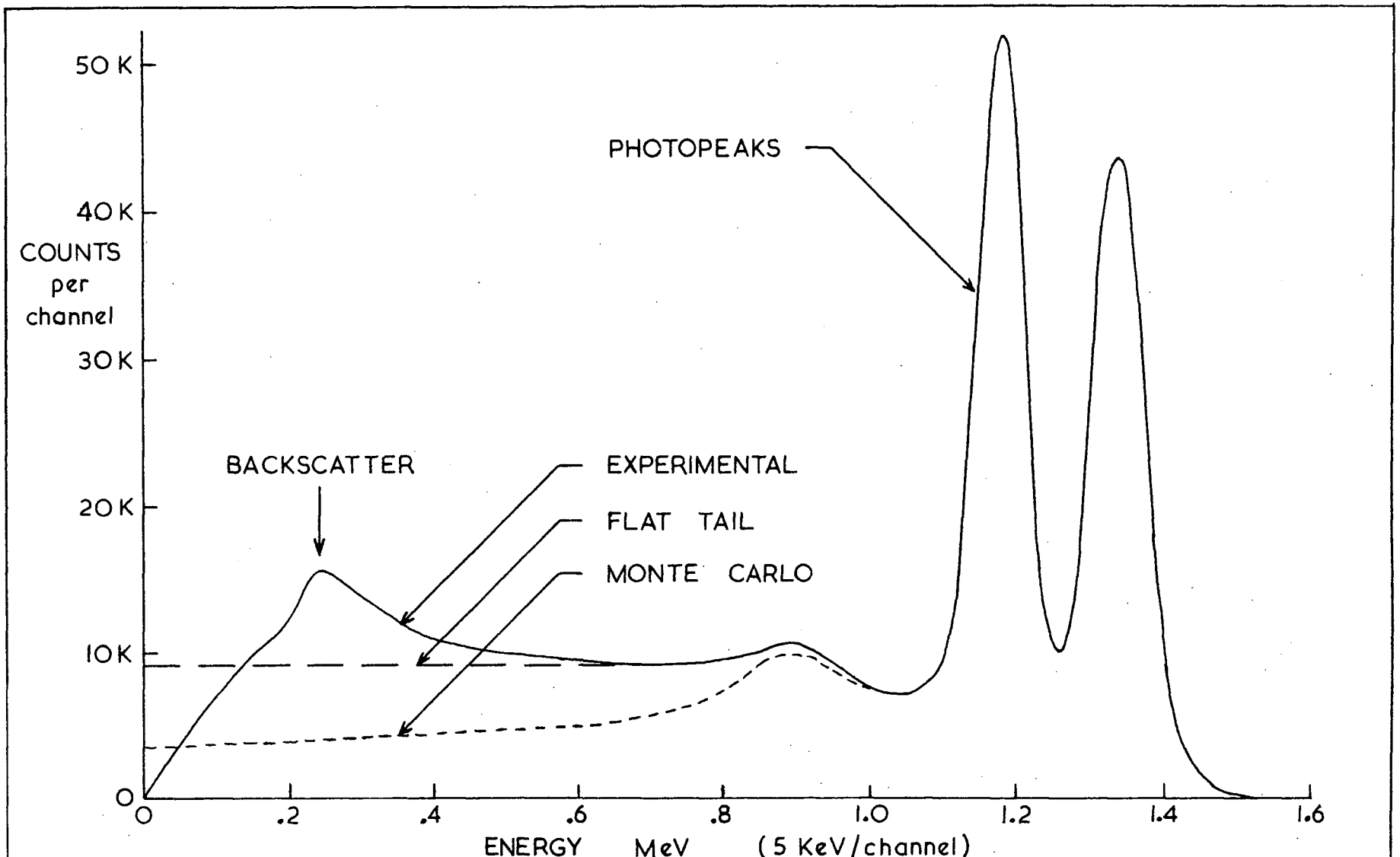

FIGURE 8. Experimental spectrum from the Co-60 source #15 with background removed. The run time was two hours. The two approximations to the tail shape are the flat tail and Monte Carlo shapes.

was $(1.14 \pm 0.02) \times 10^{-2}$. These values are in good agreement, confirming the summation hypothesis stated above, which depends on the fact that the free spectrum (after background subtraction) should have the same shape as the coincidence spectrum.

4.6 Efficiency Measurements with the Standard Source

The calibrated Co-60 source supplied by the International Atomic Energy Agency (hereafter denoted IAEA) was stated to be 10.78 ± 0.21 microcuries on January 1, 1967. Using a half life of 5.27 ± 0.05 years for the decay, the source strength corrected to May 5, 1967, was found to be 10.3 ± 0.3 microcuries.

Because of the high counting rate from this stronger source in the same geometry as for the previous weaker sources, the experimental configuration was modified for these measurements. Of two parallel outputs from the detector preamplifier, one was fed directly to the internal amplifier of the ND 160 kicksorter, while the second went to a double delay line amplifier, single channel analyzer, and scaler, with a total resolving time of less than 4 microseconds. The window of the single channel analyzer was set to correspond to an energy range of 0.8 to 1.6 MeV, eliminating the lower part of the spectrum, in order to reduce the count rate in the scaler. With these settings, the scaler count rate was 3×10^5 (including 1.5×10^3 background) counts per minute. The kicksorter count rate was

5×10^5 counts per minute, of which 7×10^3 counts per minute were background, with a dead time of 50 percent. This large dead time is not known accurately enough to interpret the counting rate accurately on a quantitative basis, however according to the manufacturer such large dead times should not significantly modify the spectrum shape. The number of counts in the total spectrum was deduced from the scaler counts, using the ratio of counts between 0.8 and 1.6 MeV to the total spectrum counts as obtained from the kicksorter spectrum.

The pulse pile-up corrections, using a resolving time of 2 microseconds, totaled 4.5 percent for the kicksorter. The resolving time of the scaler circuit was determined from the width of the double differentiated pulse from the amplifier to be 1 microsecond. The total pile-up correction for the scaler circuit was 3 percent.

On a three minute run, the total efficiency $(\epsilon_{1.173} + \epsilon_{1.333})$ was found to be $(2.13 \pm 0.04) \times 10^{-2}$, not including the pulse pile-up error, while the theoretical estimate was 1.90×10^{-2}. The 12 percent discrepancy between experiment and theory is considerably lower than the 20 percent discrepancy obtained in the coincidence method. This is at first sight rather disturbing, since one would expect that essentially the same factors which caused the discrepancy between theory and experiment in one case should be operative in the other. However, the systematic pulse pile-up error of about 7.5 percent

lowers the discrepancy to within the other experimental and statistical uncertainties.

4.7. Results at 1.173 and 1.333 MeV with no Collimators on the Counters

Coincidence Method I and the standard source method were used to measure the efficiencies of the detectors with the collimators removed. For the coincidence method and source #11, the free count rate was 5×10^4 counts per minute, of which 10^4 counts per minute were background, and the coincidence rate was 10^3 counts per minute, including 25 counts per minute of random counts. The pulse pile-up effects for these count rates were 1.5 percent in the kicksorter. Spectra taken with and without the collimator, normalized to equal kicksorter live times of 16 minutes, are shown in Figure 9 to illustrate the effect of the collimator.

For a 15 minute run using source #11, the average efficiency was found to be

$$\frac{N_c}{N_1 F(\theta)} = \frac{2\epsilon_{1.173}\,\epsilon_{1.333}}{\epsilon_{1.173} + \epsilon_{1.333}} = (2.30 \pm 0.05) \times 10^{-2}$$

where the pulse pile-up corrections were not included. The theoretical value of this parameter is 1.60×10^{-2}. The 43 percent difference here is to be compared with the 22 percent deviation of the measurement made with the collimators on the counters. The reason for these differences is discussed in Chapter VI, which deals with spectrum shapes.

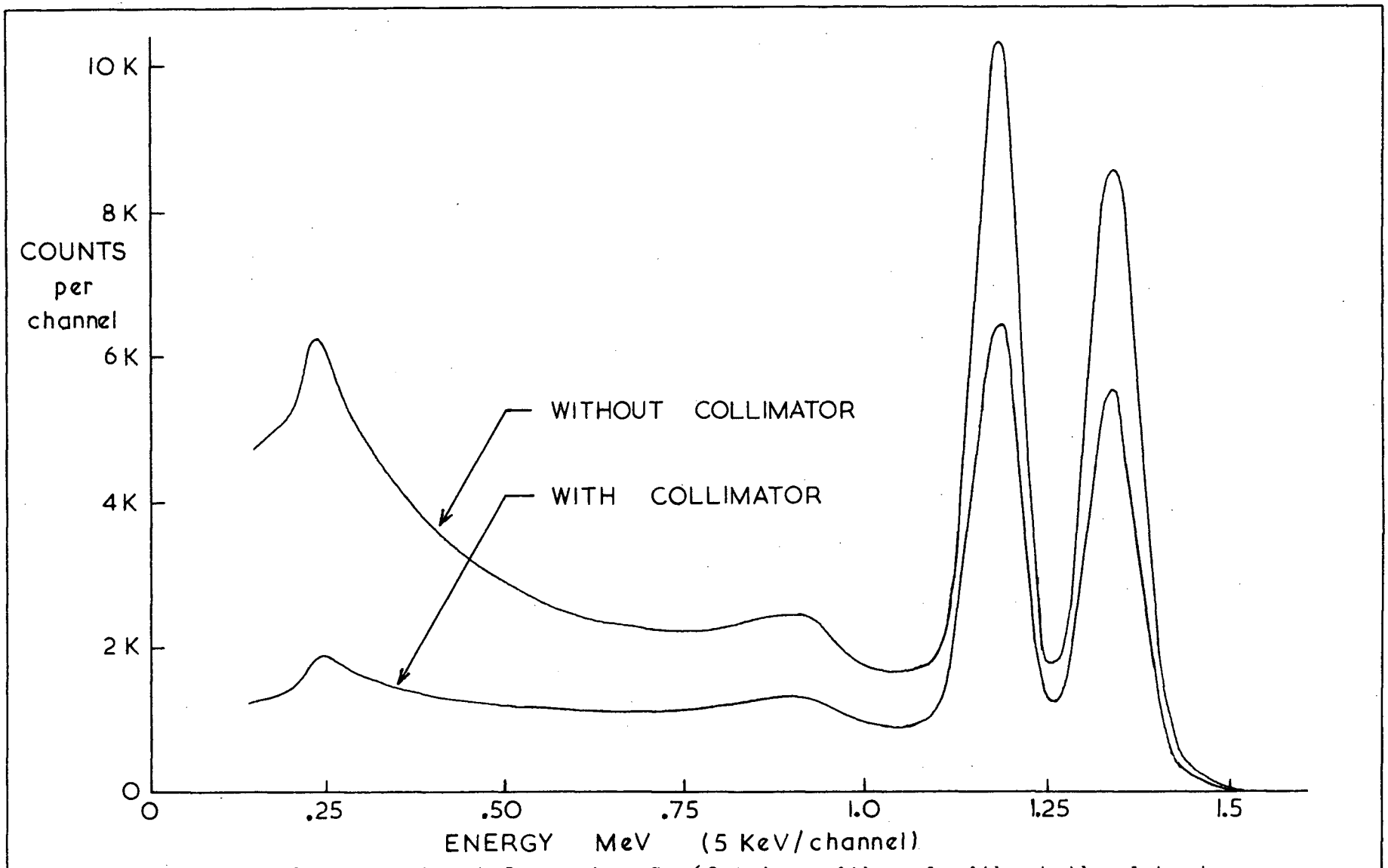

FIGURE 9. Experimental spectra Co-60 taken with and without the detector collimators, with the backgrounds removed. The spectra are normalized to equal live times of 16 minutes, using source #15.

In the standard source method described in the previous section, the single channel analyzer window covered the equivalent energy range of 1.0 to 1.6 MeV. Counting rates of 10^6 counts per minute, of which 10^4 counts per minute were background, with a dead time of 60 percent were observed in the kicksorter. The count rate of 4×10^5 counts per minute (10^3 counts per minute background) was observed in the scaler. The pulse pile-up error in kicksorter was 9 percent, the pulse pile-up error in the scaler system was 3 percent.

In the three minute run the total efficiency ($\epsilon_{1.173} + \epsilon_{1.333}$) with no pile-up correction was $(3.86 \pm 0.09) \times 10^{-2}$. For the coincidence method, the corresponding deviation was 43 percent. The difference in the percent deviations is only partly explained here by the pulse pile-up effect. A second source of systematic error is the dead time in the double delay line amplifier. This dead time, based on a resolving time of 1.5 microseconds, is about 4 percent. Also, the large kicksorter dead time, and significant pulse pile-up effect, may possibly have caused a slight distortion in the kicksorter spectrum shape.

CHAPTER V

SOURCE STRENGTH DETERMINATIONS

5.1. The Theory

An absolute calibration of the strengths of the Co-60 sources used in the experiment has been done both by using the data available from the Coincidence Method I, and by inter-comparison with the IAEA standard source.

A useful by-product of the Coincidence Method I discussed in Section 3.1 is that the strength of the source used in a measurement can be found, almost independent of the counter efficiencies. From Section 3.1 the relevant equations for identical counters are:

$$N_1 = N_2 = (\epsilon_{11} + \epsilon_{21}) N_o \qquad (5.1)$$

$$N_c = 2 \epsilon_{11} \epsilon_{21} N_o F(\theta) \qquad (5.2)$$

Upon division of equation (5.2) by the square of equation (5.1) the result is:

$$\frac{N_c}{N_1^2} = \frac{2 \epsilon_{11} \epsilon_{21} F(\theta)}{(\epsilon_{11} + \epsilon_{21})^2 N_o}$$

$$N_o = \frac{N_1^2 F(\theta)}{N_c} \left(\frac{2 \epsilon_{11} \epsilon_{21}}{(\epsilon_{11} + \epsilon_{21})^2} \right)$$

For most gamma-ray energies, the values of the factor $2 \epsilon_{11} \epsilon_{21} / (\epsilon_{11} + \epsilon_{21})^2$ are insensitive to the numerical values of the counter efficiencies. The values of the efficiency factor shown in Table 9 are based on either the measure-

ments of the previous chapter, or the theoretical efficiencies calculated using the total absorption cross sections. The example "worst case" is for gamma-rays of 0.1 and 6.0 MeV, and represents the minimum value of the efficiency dependent factor for the gamma-ray energy range 0.1 to 20 MeV.

TABLE 9.

Values of the Efficiency Factor

Source of Efficiency Values	Value of Factor
$\epsilon_{11} = \epsilon_{21}$	0.500
ϵ_{11} and ϵ_{21} from theory	0.500
ϵ_{11} and ϵ_{21} from experiment	0.53±0.04
ϵ_{11} and ϵ_{21} "worst case"	0.472

When the standard source is used, the source strengths found are completely independent of counter efficiency, since ratios of counts are used. The relevant ratio is

$$\frac{S_1}{N_1} = \frac{S_2}{N_2}$$

where S_i is the strength of source i and N_i is the count rate observed for that source.

5.2. Experimental Results of Source Strength Measurements

Two Co-60 sources, #11 and #15, were measured by the

coincidence method. These two sources, as well as that labelled #1, were measured relative to the IAEA standard source mentioned earlier. Source #1 is of interest here since it was calibrated to be 23.7±0.6 microcuries of April 22, 1958 (Singh, 1959). Using the 5.27±0.05 year half life for the Co-60 isotope, the strengths of the calibrated sources were corrected for decay as of May 5, 1967, giving the values

IAEA standard	10.3 ± 0.2 microcuries
U.B.C. #1	7.2 ± 0.25 microcuries.

In the standard source experiments, a single electronic channel consisting of a double delay line amplifier, single channel analyzer, and scaler was used for data acquisition. The single channel analyzer was set for the energy range 0.8 to 1.6 MeV, eliminating the lower part of the spectrum in order to reduce the experimental count rates. The counts in this energy region, taken in three minute runs, were compared for the various sources. Pulse pile-up corrections were not made.

The results for all the source strength determinations are shown in Table 10.

TABLE 10.

Results of Source Strength Measurements

Source	Strength from Coincidence Method	Strength from Comparison to Standard	Percent Difference Between Methods
# 1	n.a.	7.0 ± 0.2 μc	n.a.
#11	0.47 ± 0.01 μc	0.42± 0.02 μc	11 %
#15	0.64 ± 0.02 μc	0.59± 0.02 μc	8 %

Since source #1 is about the same strength as the calibrated IAEA source, the pulse pile-up effects will be the same for the two sources. Thus, the source strength measured for #1 by comparison to the standard shows good agreement with the previous calibration of 7.2 ± 0.25 microcuries. The estimated pulse pile-up corrections of 3 percent in the scaler for the standard source method (see Section 4.6) raises the values of the source strengths of sources #11 and #15 to just within the uncertainties due to the other experimental and statistical effects.

CHAPTER VI

REMARKS ON SPECTRUM SHAPE

6.1. The Effects of Spectrum Shape on the Measured Efficiency

Various experimental effects combine to cause the measured detector efficiency to be higher than that expected from the total absorption theory. The lead shielding and, to some extent, the collimator cause gamma-rays not initially incident on the NaI(Tl) crystal solid angle to be scattered into the crystal, where they are detected. Also, secondary photons from other effects in the surrounding material can be detected in the crystal. The presence of material behind the NaI(Tl) crystal is noted by the backscatter peak at 250 KeV (see Figure 8). Here gamma-rays that pass through the crystal are scattered, and the secondary products of this interaction are subsequently detected in the crystal.

The extra counts, when included in the spectrum integrations, produce a high value of the measured efficiency compared to the theoretical efficiency estimates. In the coincidence methods, such counts can also contribute to the true coincidence spectrum. These events could be accounted for only by approximate methods based on some interpretations of the spectrum shapes. These effects are verified in the Co-60 results taken with and without the collimators. The presence of many low energy counts in the no collimator case

causes the measured efficiency to be much higher, relative to the theoretical estimate, then in the case using the collimator.

It is not surprising, then, that the measured values of efficiency are found to be high relative to the theory. The results from the B^{11}+ p reaction are much higher, relatively, than the Co-60 results. This may be caused by the use of the flat tail approximation and/or the higher gamma-ray energies. Possibly more massive collimators would lessen the energy dependence of the collimator.

In his thesis, Leigh (1964) devotes one chapter to relating the observed spectrum shapes to hypothetical shapes which give, upon analysis, efficiency values in agreement with those calculated using the total absorption theory. There is no rigorous way of defining the appropriate shapes, other than using a Monte Carlo method of estimating the probable gamma-ray interactions in the crystal. Such Monte Carlo methods are difficult to use, in terms of the vast amount of calculation necessary to follow each gamma-ray through several interactions in the crystal.

In the following discussion, the term standard curve will be taken to mean the curve which, when normalized to the photopeak of an experimental spectrum, would give the same detector efficiency as that predicted by the absorption theory.

Such a curve appears in the Co-60 spectrum of Figure 8; this curve was estimated from a similar diagram in Leigh (1964). In an experimental situation, the standard curve would be applied to a spectrum to give the 'true' number of counts in that spectrum, as predicted by the theoretical efficiency estimates. Using the integrated counts from the standard curve, and the theoretical efficiencies, the absolute gamma-ray fluxes in the experiment are immediately known.

The author feels that the derivation of a set of standard curves would prove useful, and that they would be independent of the counter geometry used in the experiments. As an illustration, the results of Chapter IV are compared in Table 11.

TABLE 11.

Comparison of Results With and Without Collimator

Geometry	Measured Efficiency	Theoretical Estimate	Percent Deviation
collimator	$(1.15 \pm 0.02) \times 10^{-2}$	9.51×10^{-3}	20%
no collimator	$(2.30 \pm 0.05) \times 10^{-2}$	1.60×10^{-2}	43%

The relative error changes in the two cases. However, the larger error in the no collimator case may be due to the larger proportion of low energy counts in the spectra from the no collimator case.

Comparison of the flat tail approximation and the experimental and standard curves of Figure 8 show that here the flat tail approximation will yield efficiency values close to the experimental values. The relationship between the experimental values of efficiency, the values from the flat tail approximation, and the theoretical estimates, depend critically on the counter geometry and the gamma-ray energy. It is clear that, for lack of further information, the flat tail is a reasonable first approximation to the experimental spectrum tails.

6.2. Spectrum Separation Experiments

Several attempts were made to separate the superimposed contributions of several gamma-rays by subtracting two spectrum shapes. Provided that the energies of two gamma-rays in a cascade are not too close together, Coincidence Method II (Section 3.2) can be used to observe the separated spectrum of the lower energy gamma-ray. In principle this "shape" can be normalized and used to exactly cancel out the same component of a free spectrum, leaving a separated spectrum of the higher energy gamma-ray.

Experimentally, such methods were applied to both the Co-60 and B^{11} + p spectra. The results achieved were not promising; the several problems encountered are outlined below:

(a) The spectrum shape to be subtracted from the total had to have excellent channel by channel statistics. For normal coincidence count rates, this meant prohibitively long

counting times. For slowly varying regions of the spectra, the statistical criterion was less stringent, but the matching of peak shapes was difficult.

(b) The electronic stability of the preamplifiers and kicksorters varied slowly during counting times of several hours. This tended to broaden the spectrum peaks of the coincidence spectrum, so that a true spectrum shape was not obtained. Gain changes of one or two channels in one hundred during a several hour long counting run changed the peak shapes significantly.

(c) The gain and energy zero of the two spectra to be subtracted had to be closely matched. In practice the gain of the spectrum to be subtracted was arbitrarily varied to give the best peak cancellation; this was a tedious process.

The spectrum subtraction concept was successfully applied in one case. The reaction $F^{19}(p\,\alpha\,\gamma)O^{16}$ produces a strong gamma-ray line at 6.14 MeV, with no strong interfering lines down to about 1.2 MeV. The shape of this spectrum, taken with the same counter geometry, was gain shifted to represent the 6.48 MeV gamma-ray line of the B^{11} + p spectrum. To the accuracy required here, the contribution of this gamma-ray line was completely removed. Still, however, nothing could be said about the spectrum shapes below 1.2 MeV.

CHAPTER VII

TRIPLE CORRELATIONS IN THE $B^{11}(p\gamma\gamma)\,C^{12}$ REACTION

7.1. Introduction

A literature review, based on the 1959 and 1962 compilations of Ajzenberg-Selove and Lauritsen, revealed that few definite results were available concerning measurements of triple correlations in the $B^{11}(p\gamma\gamma)C^{12}$ reaction. Since at least one of the correlation functions was required to complete the efficiency measurements, efforts were made to investigate the correlation.

7.2. The Theory of the Triple Correlation

The theoretical estimates were made using the angular correlation theory of Ferguson (1965). No attempt will be made to derive the theory here; the general results for particle-gamma-gamma correlations given by Ferguson will be quoted. The general results are then applied to the $B^{11}(p\gamma\gamma)C^{12}$ reaction and evaluated for the desired geometries. The problem is set up as follows.

In general the beam direction and the positions of the two counters are specified by the angle pairs $\Omega_i = (\theta_i, \phi_i)$ with respect to a fixed laboratory co-ordinate system centered at the target. The correlation results are much simpler if the incoming beam direction defines the positive z-axis of this co-ordinate system. In this case the two angles Θ_2 and

θ_3 and the relative azimuthal angle ϕ describe the system completely.

The spins and angular momenta are best illustrated by a diagram (see Figure 10).

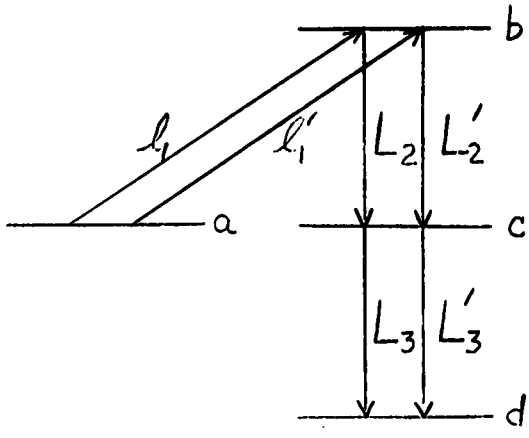

FIGURE 10: Levels, spins and angular momenta in a (p $\gamma\gamma$) reaction.

The primed quantities refer to competing channels in the reaction. The proton with orbital angular momentum $\underline{l}_1$ (or $\underline{l}_1'$) couples with the channel spin $\underline{a}$ to form a compound state of spin $\underline{b}$. This state emits a multipole $\underline{L}_2$ (and/or $\underline{L}_2'$) to form the intermediate state $\underline{c}$. The second gamma-ray, $\underline{L}_3$ and/or $\underline{L}_3'$, is emitted, leaving the final state of spin $\underline{d}$.

The following three angular momenta can be defined in terms of the angular momenta associated with the two radiative transitions.

$$\begin{aligned} \underline{k}_1 &= \underline{k}_2 + \underline{k}_3 \\ \underline{k}_2 &= \underline{L}_2 + \underline{L}_2' \\ \underline{k}_3 &= \underline{L}_3 + \underline{L}_3' \end{aligned} \qquad (7.1)$$

The angular correlation between the radiations emitted by the two transitions can then be defined in terms of general angular momentum functions given by Ferguson.

$$X^{\kappa}_{k_2 k_3}(\theta_2 \theta_3 \phi) = \hat{k}_2 \hat{k}_3 \left[\frac{(k_2-\kappa)!(k_3-\kappa)!}{(k_2+\kappa)!(k_3+\kappa)!}\right]^{1/2} P^{\kappa}_{k_2}(\cos\theta_2) \cdot P^{\kappa}_{k_3}(\cos\theta_3)\cos\kappa\phi \quad (7.2)$$

$$P_{k_1 k_2 k_3}(\theta_2 \theta_3 \phi) = \frac{i^{k_1+k_2-k_3}}{\hat{k}_2 \hat{k}_3^2} \sum_{\kappa \geq 0}^{\min(k_2 k_3)} (2-\delta_{\kappa 0})(k_1 0 k_2 \kappa | k_3 \kappa) \cdot X^{\kappa}_{k_2 k_3}(\theta_2 \theta_3 \phi) \quad (7.3)$$

Here the $P^m_\ell(\cos\theta)$ are Associated Legendre Polynomials, and $\hat{x}$ is given by $\hat{x} = (2x + 1)^{\frac{1}{2}}$. It should be noted here that the counter situated at angle θ_2 detects the multipole L_2, and the counter at angle θ_3 detects the multipole L_3.

At this stage further geometrical simplifications are used. If one or more of the angles θ_2, θ_3 or ϕ are set equal to 90°, then the $X^{\kappa}_{k_2 k_3}(\theta_2 \theta_3 \phi)$ vanish for odd κ. If either θ_2 or θ_3 is 0° or 180° all $X^{\kappa}_{k_2 k_3}(\theta_2 \theta_3 \phi)$ vanish for non-zero κ. The procedure here is to set one of the counters at a convenient angle, and vary the position of the second counter in the plane defined by the first counter and the beam direction. Therefore the angular dependence is reduced to a single variable θ, the position of the movable counter with respect to the forward beam direction. Assuming these conditions we have:

$$W^{(i)}(\theta) = \sum_K a_K^i \, P_K(\cos\theta) \tag{7.4}$$

$$a_K^i = \frac{1}{(4\pi)^3} \sum_{\mu} \Big[(-1)^{a+d} \hat{a}^{-2} \bar{Z}(\ell_1 b \ell_1' b; a k_1) \, G_\gamma \begin{Bmatrix} c & L_2 & b \\ c & L_2' & b \\ k_3 & k_2 & k_1 \end{Bmatrix} \cdot$$

$$\bar{Z}_1(L_3 c L_3' c; d k_3) \langle b \| \ell_1 | a \rangle \langle b \| \ell_1' | a \rangle^* \langle c | L_2 \| b \rangle \cdot$$

$$\langle c | L_2' \| b \rangle^* \langle d | L_3 \| c \rangle \langle d \| L_3' | c \rangle^* Q_{k_2} Q_{k_3} \alpha^i_{k_1 k_2 k_3 K} \Big] \tag{7.5}$$

$$P_{k_1 k_2 k_3}(\theta_2 \theta_3 \phi) = \sum_K \alpha^i_{k_1 k_2 k_3 K} \, P_K(\cos\theta) \tag{7.6}$$

Here the angular correlation for a specific geometry (i) is given by $W^{(i)}(\theta)$. In equation (7.5), the expression for a_k^i, the summation symbol μ implies a summation over all allowed values of the parameters a, ℓ_1, ℓ_1', L_2, L_2', L_3, L_3', k_1, k_2, k_3. Ferguson tabulates the values of the $\alpha^i_{k_1 k_2 k_3 K}$ for several specified geometries, but the values required here were evaluated from equations (7.2), (7.3), and (7.6).

The values of the various coefficients $\bar{Z}$, $\bar{Z}_1$, G_γ, the 9-j symbol, and the Clebsch-Gordon coefficients were found from the literature tabulations (Ferguson, 1965, and Sharp et al, 1961). The reduced matrix elements, for the B^{11}+p reaction, constitute a constant normalization factor in front of the entire correlation function, hence they will not be rigorously defined here. The Q_{k_i} terms are the corrections for

the finite counter solid angle (see Appendix C).

The general procedure used in the solution of this problem is outlined in the following steps:

(a) The required values of the angular momenta concerned in the B^{11} + p reaction were found from the literature.

(b) Parameters having unique values were substituted directly into the equations (7.2) to (7.6). Allowable values of the remaining parameters were defined.

(c) Equations (7.2) and (7.3) were evaluated to give the function $P_{k_1 k_2 k_3}(\theta_2 \theta_3 \phi)$ as a sum of Associated Legendre Polynomials.

(d) Specific assumptions about the counter geometry were inserted into equation (7.3), and the $P_{k_1 k_2 k_3}(\theta_2 \theta_3 \phi)$ reduced to a sum of ordinary Legendre Polynomials. The summation was compared to equation (7.6) to give numerical values for the $\alpha^{i}_{k_1 k_2 k_3 K}$ coefficients.

(e) The values of $\alpha^{i}_{k_1 k_2 k_3 K}$ were substituted into equation (7.5). Evaluation of this equation gave the a^{i}_{k}, the required coefficients in the angular correlation function (7.4).

For the B^{11} + p reaction, the angular momenta and spins allowed are tabulated in Table 12 (data from Ajzenberg-Selove and Lauritsen, 1959).

TABLE 12.

Allowed Spins and Angular Momenta in the B^{11} + p Reaction

Definition	Symbol	Values
spin and parity of target	s_1^{π}	$3/2^-$
spin of proton	s_o	1/2
orbital angular momentum of proton	ℓ_1, ℓ_1'	1
spin and parity of compound level	b^{π}	2^+
spin and parity of intermediate level	c^{π}	2^+
spin and parity of final level	d^{π}	0^+
1st emitted multipole (11.68 MeV)	L_2, L_2'	1
2nd emitted multipole (4.43 MeV)	L_3, L_3'	2

Note that we are neglecting a small interference (Ajzenberg-Selove and Lauritsen, 1959) arising from a broad S-wave resonance ($\ell_1' = 0$) at 1.388 MeV.

From the equations (7.1), the allowed values of the k_i are:

$$k_1 = 0,1,2$$
$$k_2 = 0,1,2$$
$$k_3 = 0,1,2,3,4$$

However all the states of C-12 involved in the present reaction have positive parity, therefore the k's can have only even values.

Equations (7.2) and (7.3) are now evaluated explicitly to give:

$$P_{000} = 1$$

$$P_{202} = \frac{1}{\sqrt{5}} P_2(\cos\theta_2) \qquad (7.7)$$

$$P_{220} = \frac{1}{\sqrt{5}} P_2(\cos\theta_3)$$

$$P_{022} = \frac{1}{\sqrt{5}}\left\{P_2(\cos\theta_2)P_2(\cos\theta_3) + \frac{1}{5}P_2'(\cos\theta_2)P_2'(\cos\theta_3)\cos\phi + \frac{1}{12}P_2^2(\cos\theta_2)P_2^2(\cos\theta_3)\cos 2\phi\right\}$$

$$P_{222} = \sqrt{\frac{2}{35}}\left\{P_2(\cos\theta_2)P_2(\cos\theta_3) - \frac{1}{6}P_2'(\cos\theta_2)P_2'(\cos\theta_3)\cos\phi - \frac{1}{12}P_2^2(\cos\theta_2)P_2^2(\cos\theta_3)\cos 2\phi\right\}$$

$$P_{224} = \sqrt{\frac{2}{35}}\left\{P_2(\cos\theta_2)P_4(\cos\theta_3) + \frac{1}{6}P_2'(\cos\theta_2)P_4'(\cos\theta_3)\cos\phi + \frac{1}{72}P_2^2(\cos\theta_2)P_4^2(\cos\theta_3)\cos 2\phi\right\}$$

At this stage we appeal to the specialized geometry to reduce the above equations. Figure 11 is a schematic diagram of the experimental angles used.

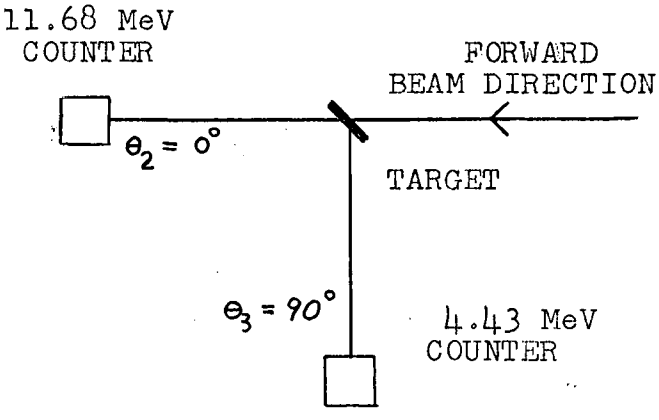

FIGURE 11. Counter positions in the B^{11} + p experiments.

It is interesting to note that this configuration applies to two angular correlation functions. The first is for θ_2 fixed at 0° and θ_3 variable (set at 90° here). The second is for θ_3 fixed at 90° and θ_2 variable (set at 0°

here). Both these angular correlation functions are evaluated theoretically and experimentally.

We now consider the case where θ_2 is fixed at zero degrees. The Associated Legendre Polynomials are:

$$P_m^n(\cos\theta)\Big|_{\theta=0^\circ} = \delta_{no}$$

Using this relationship, the equations (7.7) reduce to (where $\theta = \theta_3$):

$$\begin{aligned} P_{000} &= 1 \\ P_{202} &= \frac{1}{\sqrt{5}} P_2(\cos\theta) \\ P_{220} &= \frac{1}{\sqrt{5}} \\ P_{022} &= \frac{1}{\sqrt{5}} P_2(\cos\theta) \\ P_{222} &= \sqrt{\frac{2}{35}} P_2(\cos\theta) \\ P_{224} &= \sqrt{\frac{2}{35}} P_4(\cos\theta) \end{aligned} \qquad (7.8)$$

Comparison of the numerical coefficients of these equations with the $\alpha^i_{k_1 k_2 k_3 K}$ from equation (7.6) gives values of the $\alpha^i_{k_1 k_2 k_3 K}$ which agree with those tabulated by Ferguson.

From Table 12 we see that the values of channel spin are a = 1, 2. Using the reduced matrix elements from equation (7.5) we define the channel spin ratio R by

$$R = \frac{\left[|\langle b\|\ell_1|a\rangle|^2\right]_{a=2}}{\left[|\langle b\|\ell_1|a\rangle|^2\right]_{a=1}} \qquad (7.9)$$

Using equations (7.4) and (7.5) and tabulated values of the $\bar{Z}$, $\bar{Z}_1$, G_γ, and 9-j coefficients we arrive at the final expression

$$W^{(1)}(\theta) = a_0 + a_2 P_2(\cos\theta) + a_4 P_4(\cos\theta) \qquad (7.10)$$

where

$$\begin{aligned} a_0 &= M\{\, 0.2462\, R + 0.3488\} \\ a_2 &= M\{\, 0.03770\, R + 0.03367\} \\ a_4 &= M\{-0.002160\, R + 0.002788\} \end{aligned} \qquad (7.11)$$

Here M is a normalization factor containing squares of the reduced matrix elements, i.e.

$$M = \frac{1}{(4\pi)^3} \langle b\|l_1\|a\rangle \langle b\|l_1'\|a\rangle^* \langle c|L_2\|b\rangle \langle c|L_2'\|b\rangle^* \langle d|L_3\|c\rangle \langle d|L_3'\|c\rangle^*$$

By our definition of the channel spin ratio (equation (7.9)), we require a = 1 in this expression. Numerically M becomes

$$M = \frac{1}{(4\pi)^3} |\langle 2\|1\|1\rangle|^2 |\langle 2|1\|2\rangle|^2 |\langle 0|2\|2\rangle|^2$$

which is a constant.

Now we evaluate the second case, namely $\theta_3 = 90^\circ$ and $\theta_2 = \theta$. Here we have

$$\begin{aligned} P_m^n(\cos\theta)\Big|_{\theta=90^\circ} &= \frac{(-1)^p (2p+2m)!}{2^n\, p!\,(p+m)!} && \text{if } m-n = 2p \\ &= 0 && \text{if } m-n = 2p+1 \end{aligned}$$

After inserting these values into the set of equations (7.7) we get expressions involving the polynomial $P_2^2(\cos\theta)$. This

is reduced using the result

$$P_2^2(\cos\theta) = 2\left[1 - P_2(\cos\theta)\right]$$

Then we have the following equations for the $P_{k_1 k_2 k_3}$:

$$\begin{aligned} P_{000} &= 1 \\ P_{202} &= \frac{-1}{2\sqrt{5}} \\ P_{220} &= \frac{1}{\sqrt{5}} P_2(\cos\theta) \\ P_{022} &= \frac{1}{2\sqrt{5}}\left[1 - P_2(\cos\theta)\right] \\ P_{222} &= \frac{-1}{\sqrt{70}} \\ P_{224} &= \frac{1}{12\sqrt{70}}\left[14\, P_2(\cos\theta) - 5\right] \end{aligned} \tag{7.12}$$

Using the same procedure as before we arrive at the angular correlation function

$$W^{(2)}(\theta) = a_0 + a_2 P_2(\cos\theta) \tag{7.13}$$

where

$$\begin{aligned} a_0 &= M\{0.2717 R + 0.3571\} \\ a_2 &= M\{-0.04470 R - 0.02463\} \end{aligned} \tag{7.14}$$

for the same definition of M as before.

As mentioned previously, the two correlation functions, equations (7.10) and (7.13), must agree for specified angles. That is

$$W^{(1)}(\theta)\Big|_{\theta=90^\circ} = W^{(2)}(\theta)\Big|_{\theta=0^\circ}$$

Evaluation of this expression shows that the relationship holds within the accuracy of the calculations, independent of the value of the channel spin ratio R.

In the experiment to be described later, measurements were made for the second of the two cases derived here. The zero-to-ninety degree ratio of the correlation was measured, for the angle θ_3 fixed at 90° degrees (see Figure 11). Some equations relating this ratio to the functions derived above are now discussed.

If the correlation has the form

$$W(\theta) = a_0 + a_2 P_2(\cos\theta) \tag{7.15}$$

then the zero-to ninety ratio X is (assuming the a_i have been corrected for finite counter solid angle)

$$X = \frac{W(0°)}{W(90°)} = \frac{a_0 + a_2}{a_0 + \frac{1}{2}a_2}$$

After inversion, this result becomes

$$\frac{a_2}{a_0} = \frac{X-1}{1-\frac{1}{2}X} \tag{7.16}$$

Now, from Appendix B, the function $F(\theta)$ required in the efficiency measurements is

$$F(\theta) = 1 + \frac{a_2}{a_0} P_2(\cos\theta)$$

Since $\theta = 0°$ in the experiments done

$$F(0°) = 1 + \frac{a_2}{a_0}$$
$$F(0°) = \frac{3X}{2+X} \tag{7.17}$$

Using equations (7.13) to (7.16), the channel spin ratio R becomes related to the zero-to-ninety degree ratio X by the following formula:

$$R = \frac{0.3694X - 0.3325}{0.2270 - 0.2940X} \tag{7.18}$$

Unfortunately, equation (7.18) exhibits singular behaviour for values of X in the region of interest. Specific-

ally, R = 0 when X = 0.90 and R = ∞ when X = 0.772. Therefore a small uncertainty in a zero-to-ninety degree ratio value in this region forces a large uncertainty in the resulting channel spin ratio value.

7.3. Experimental Investigations of the Correlation Functions

Experimentally, a measurement of the zero-to-ninety degree ratio of the correlation function values was made to check the theoretical results. Also, this measurement provided a value of the factor required for the efficiency results that was independent of the theoretical correlation functions.

The counter detecting the 4.43 MeV radiation was fixed at $\theta_3 = 90^\circ$, and the second counter (detecting 11.68 MeV gamma-rays) was placed at the angles $\theta_2 = 0^\circ$ and $\theta_2 = 90^\circ$ for the ratio measurement. The value of the zero-to-ninety degree ratio was found to be 0.88 $\pm$ 0.02. From the correlation function quoted by Hubbard et al (1952), the value of the ratio is 0.875 $\pm$ 0.06. Assuming a channel spin of 0.42 $\pm$ 0.02 (Grant et al, 1954) and the function derived in Section 7.2, the zero-to-ninety degree ratio becomes 0.907 $\pm$ 0.002. These three values show good agreement.

Using the experimental zero-to-ninety degree ratio, the numerical values of the angular correlation function coefficients were found. From equation (7.18) the channel spin ratio was found to be

$$R = 0.28 \pm 0.28$$

while other measurements of this parameter are

$R = 0.42 \pm 0.02$ Grant et al, 1954

$R = 0.52 \pm 0.03$ Craig et al, 1956

Using the zero-to-ninety degree ratio directly, the second correlation function (4.43 MeV counter fixed at 90° to the forward beam direction) becomes

$$W^{(2)}(\theta) = 1.0 - (0.12 \pm 0.02)\ P_2(\cos\theta)$$

which compares favourably with the function

$$W^{(2)}(\theta) = 1.0 - (0.125 \pm 0.06)\ P_2(\cos\theta)$$

reported by Hubbard et al (1952).

From the present experimental value of the channel spin ratio, the first correlation function (11.68 MeV counter fixed at 0° to the beam direction) was found to be

$$W^{(1)}(\theta) = 1.0 + (0.10 \pm 0.03)\ P_2(\cos\theta) + (0.005 \pm 0.002)\ P_4(\cos\theta)$$

Clearly, the measurement of two points on the correlation curve is inadequate to specify a value of the channel spin ratio. The correlation function coefficients are quite insensitive to changes in the channel spin ratio value, so that the uncertainties in the numerical coefficient values found here are not excessively large. The correlation functions investigated above contain some error, because the slight interferences due to S-wave capture of the proton by the B-11 nucleus was not included in the analysis. In spite of this, the present measurements agree with those quoted in the literature.

CHAPTER VIII

CONCLUSIONS

Efficiencies measured by taking all the counts in the spectra were significantly higher than theoretical efficiency estimates based on total absorption cross sections. The magnitude of this difference depends on the geometry of the collimators and shields and on the gamma-ray energy. For both gamma-ray cascades studied, two independent methods were used to determine counter efficiency. The results of the two methods used for the 4.43 MeV and 11.68 MeV cascade were self-consistent. The results for the 1.173 MeV and 1.333 MeV cascade were also self-consistent, when pulse pile-up corrections were applied to the standard source results.

The results presented here are the final set from many trials. In all trials, the results were approximately the same as those discussed here.

The effect of the collimators on the spectra was as anticipated in Section 2.2. Specifically, use of the collimators lowered the ratio of low energy to high energy counts in the experimental spectra, and reduced the deviations between the experimental and theoretical efficiency estimates. The difficulties of high count rates and pulse pile-up encountered with the standard source method clearly indicate that with the present geometry significant corrections will be

required for counting rates of the order of 10^5 counts per minute or higher.

The deviation between the experimental and theoretical efficiency for the Co-60 cascade is 20 percent while for the B^{11} + p cascade it is 40 percent. A significant deviation would be expected in the direction observed, however it is not clear why the deviation is so different for the two experiments, with low and high energy gamma-rays. One possible explanation suggested by the absorption coefficients is that for the two higher energy gamma-rays (4.43 and 11.68 MeV), the absorption in the length of the NaI(Tl) crystal is only 60 percent of the absorption of the two lower energy gamma-rays (1.178 and 1.333 MeV). Furthermore, the lower absorption in the lead collimator and shield for the higher energy gamma-rays allows more scattering from the shield and collimator into the crystal. Consequently, the number of gamma-rays scattered into the crystal by the shield and collimator is a larger fraction of the number detected.

With some method of making an absolute calibration, such as by coincidence of cascade gamma-rays fluxes or by using a standard source, one can relate the total spectrum shape and number of counts to an absolute gamma-ray flux, and thus be independent of the theory. This is not always possible for the gamma-rays of interest, and when it is, the measurements are time consuming.

There are a number of published tables of efficiencies for NaI(Tl) scintillation counters based on total absorption cross sections integrated over the crystal volume. It is common to use these in interpreting experimental data to give absolute cross sections and gamma-ray fluxes for nuclear reactions. On the basis of the present work, it is clear that one cannot relate the total number of counts in a given spectrum to the number of gamma-rays entering the counter, using theoretical efficiencies, to an accuracy better than 25 or 30 percent. This value can be improved by taking into account the additional counts in the low energy regions of the spectra, which are due to gamma-rays scattered into the crystal from the shields, collimators and crystal mountings.

This work shows that the total number of counts in a spectrum always corresponds to a higher efficiency than that predicted by the total absorption theory. It is difficult, however, to specify the value of the corrections required for a general case, since the corrections depend so markedly on the shielding and collimator geometry.

APPENDIX A

THE TOTAL ABSORPTION EFFICIENCY THEORY

In the total absorption theory, the efficiency of gamma-ray detection is defined as the ratio of the number of gamma-rays losing energy in the scintillator to the number of gamma-rays emitted by the source. First we consider a small increment of the detector solid angle, $d\Omega$. Then, if N_i is the number of gamma-rays incident on $d\Omega$, the number of gamma-rays at a depth X in the crystal is given by the exponential absorption law to be

$$N = N_i e^{-\mu x}$$

here μ is the total absorption coefficient. The number of gamma-rays leaving the back face of a crystal of thickness T having lost no energy in the crystal is

$$N_e = N_i e^{-\mu T}$$

Clearly, the number of photons detected by their energy loss is

$$N_D = N_i - N_e = N_i(1 - e^{-\mu T})$$

If there is a collimator and/or an absorber, the number N_i reaching the solid angle $d\Omega$ out of N_o gamma-rays emitted by the source is

$$N_i = N_o e^{-\mu_A T_A - \mu_C T_C} \frac{d\Omega}{4\pi}$$

where μ_A, μ_C, T_A and T_C are the absorption coefficients and

thicknesses of the absorber and collimator.

Therefore the number of gamma-rays detected is

$$N_i = \frac{N_0}{4\pi} e^{-\mu_A T_A - \mu_C T_C} \left(1 - e^{-\mu T}\right) d\Omega$$

The total absorption for the detector is given by integrating this expression over the counter solid angle. It is assumed that the counters and collimators possess cylindrical symmetry about an axis going through the source of gamma-rays. We have

$$N_1 = \frac{N_0}{4\pi} \int_0^{2\pi} d\phi \int_0^{\theta_0} e^{-\mu_A T_A - \mu_C T_C} \left(1 - e^{-\mu T}\right) \sin\theta \, d\theta$$

where N_1 = total number of gamma-rays detected

θ_0 = half angle subtended by the counter face

Therefore the efficiency of the detector is

$$\epsilon = \frac{\text{number of gamma-rays detected}}{\text{number of gamma-rays emitted by the source}}$$

$$\epsilon = \frac{1}{2} \int_0^{\theta_0} e^{-\mu_A T_A - \mu_C T_C} \left(1 - e^{-\mu T}\right) \sin\theta \, d\theta$$

For the purposes of this experiment, a computer program has been written to calculate this efficiency integral by numerical methods, for any counter geometry. The geometrical measurements and absorption coefficients are input to the program. It may be noted here that the source to crystal face and source to collimator face distances are independent of the collimator shape. The program then tests the position of the

source relative to the apex of the collimator cone, and uses the appropriate calculation of gamma-ray paths in the crystal and collimator when the integration is performed.

APPENDIX B

ANGULAR CORRELATION CORRECTIONS TO EFFICIENCY MEASUREMENTS

When the two gamma-rays in a cascade are correlated as a function of the angle between their directions of emission, the number of coincidence counts obtained in two detectors will be modified by the correlation. We assume that two detectors of small solid angle are set coplanar with an angle θ between them, and that one gamma-ray is incident on one counter. We define $F(\theta)$ to be the intensity of the second gamma-ray at the angle θ, relative to an isotropic distribution. Also, we define $f(\theta)$ as the probability that the second gamma-ray will enter the second detector. Then we have

$$f(\theta)d\omega = k\sum_j a_j P_j(\cos\theta)\, d\omega$$

where k = normalization factor

$\sum_j a_j P_j(\cos\theta)$ = angular correlation function for the gamma-rays

$d\omega$ = increment of solid angle of the second detector.

This equation is now normalized to unit intensity over the sphere

$$\int_{4\pi} f(\theta)d\omega = 1 = \int_{4\pi} k\sum_j a_j P_j(\cos\theta)\, d\omega$$

Therefore

$$k = \frac{1}{4\pi a_0}$$

Then

$$f(\theta)d\omega = \frac{1}{4\pi a_0}\sum_j a_j P_j(\cos\theta)$$

For an isotropic distribution we have

$$f_1(\theta)\, d\omega = \frac{d\omega}{4\pi}$$

Therefore

$$F(\theta) = \frac{f(\theta)\, d\omega}{f_1(\theta)\, d\omega} = \frac{1}{a_0} \sum a_i P_i(\cos\theta)$$

is the desired intensity ratio. This factor $F(\theta)$ modifies the probability of a coincidence between the gamma-ray counters, as discussed in Section 3.1.

APPENDIX C

FINITE SOLID ANGLE CORRECTIONS

In an experiment where the angular distributions or correlations of gamma-rays are to be considered, the angular dependences of the functions will be smoothed by the finite angular resolution of the counters. Rose (1953) has derived the correction factors necessary to convert a measured angular dependence into the true angular dependence of any distribution or correlation. This theory is outlined here.

The detection apparatus consists of two identical scintillation counters of cylindrical geometry, with their axes intersecting at a point source of gamma-rays. If the true angular correlation is given by

$$W(\theta) = \sum_K a_K P_K(\cos\theta)$$

then the measured angular dependence is given by

$$\overline{W(\theta)} = \sum_K a_K b_K P_K(\cos\theta)$$

From this it is seen that the smoothing of the distribution changes the amplitudes of the various Legendre Polynomial contributions, but it does not give interference terms. The smoothing factors are defined by

$$b_K = \frac{J_K}{J_0}$$ for an angular distribution using one detector

$$b_K = \left(\frac{J_K}{J_K}\right)^2$$ for an angular correlation using two detectors.

where the general expression for the J_k is

$$J_K = \int_0^{\theta_0} P_K(\cos\theta)\left(1 - e^{-\mu x(\theta)}\right)\sin\theta\, d\theta$$

The factor $(1 - e^{-\mu x(\theta)})$ expresses the probability that the gamma-ray is absorbed in the counter. The integral performs the average, over the counter face, of the absorption of a gamma-ray at an angle θ with respect to the counter axis, times the relative intensity of the gamma-ray. If the counter has a collimator and/or absorber, these results hold, given the appropriate changes in the absorption function.

It is easily seen that the J_k terms are closely related to the definition of absolute detector efficiency given in Appendix A. For this reason the computer program written to evaluate the efficiencies also calculated the solid angle correction factors.

BIBLIOGRAPHY

Ajzenberg-Selove, F., and Lauritsen, T., Energy Levels in Light Nuclei, North-Holland Publishing Co., Amsterdam, 1959.

Craig, D. S., Cross, W. G., and Jarvis, R. G., Phys. Rev. 103, 1414, 1954.

Dalby, D., private communication, 1966.

Devons, S., in Proceedings of the Gatlinberg Conference 1961 on Electromagnetic Lifetimes, Nuclear Science Series Report 37, 1961.

Ferguson, A. J., Angular Correlation Methods in Gamma-Ray Spectroscopy, North-Holland Publishing Co., Amsterdam, 1965.

Grant, P. J., Flack, F. C., Rutherglen, F. G., and Deuchars, W. M., Proc. Phys. Soc. A67, 751, 1954.

Gregory, A. G., Nuclear Phys. 23, 518, 1961.

Grodstein, G. B., X-Ray Attenuation Coefficients from 10 KeV to 100 MeV, National Bureau of Standards Circular 583, 1957.

Hubbard, T. P., Nelson, E. B., and Jacobs, J. A., Phys. Rev. 87, 378, 1952.

Leigh, J. L., University of British Columbia M.Sc. Thesis, 1964.

Nuclear Data Tables 1960, National Academy of Science, and National Research Council, Washington, D.C.

Rasmussen, V. K., Metzgen, F. R., and Swann, C. P., Phys. Rev. 110, 154, 1958.

Rose, M. E., Phys. Rev. 91, 610, 1953.

Sharp, W. T., Kennedy, J. M., Sears, B. J., and Hoyle, M. G., Tables of Coefficients for Angular Distribution Analysis, CRT 556, AECL Chalk River Nuclear Project, 1961.

Siegbahn, K., ed. Alpha- Beta- and Gamma-Ray Spectroscopy, North-Holland Publishing Co., Amsterdam, 1965.

Singh, P. P., University of British Columbia PhD Thesis, 1959.